1 Title Page

Evidence for an Active Role of Inferior Frontal Cortex in Conscious Experience

Authors:

Veith Weilnhammer[1,2,*], Merve Fritsch[1,*], Meera Chikermane[1], Anna-Lena Eckert[1,4], Katharina Kanthak[1], Heiner Stuke[1,2], Jakob Kaminski[1,2], Philipp Sterzer[1,2,3,4]

Affiliations and Contribution:

[1] Department of Psychiatry, Charité-Universitätsmedizin Berlin, corporate member of Freie Universität Berlin and Humboldt-Universität zu Berlin, 10117 Berlin, Germany

[2] Berlin Institute of Health, Charité-Universitätsmedizin Berlin and Max Delbrück Center, 10178 Berlin, Germany

[3] Bernstein Center for Computational Neuroscience, Charité-Universitätsmedizin Berlin, 10117 Berlin, Germany

[4] Berlin School of Mind and Brain, Humboldt-Universität zu Berlin, 10099 Berlin, Germany

[*] Equal contribution

Corresponding Author:

Veith Weilnhammer, Department of Psychiatry, Charité Campus Mitte, Charitéplatz 1, 10117 Berlin, phone: 0049 (0)30 450 517 317, email: veith-andreas.weilnhammer@charite.de

2 Abstract

Despite a growing understanding of human brain function, it is still unclear how conscious experience emerges from neural activity. A much-debated question in the search for the neural underpinnings of consciousness is whether prefrontal cortex actively shapes conscious experience or, alternatively, serves only complementary cognitive functions such as evaluating and acting on the contents of consciousness.

Here, we studied the neural mechanisms of bistable perception to elucidate the role of prefrontal cortex in consciousness. Human participants reported periodic changes in conscious experience that were induced by conflicting sensory information. Two functional magnetic resonance imaging experiments showed that prefrontal brain activity in inferior frontal cortex signals the conflict between conscious experience and available sensory information. In a third experiment, inhibitory transcranial magnetic stimulation revealed that a disruption of neural activity in inferior frontal cortex leads to a decrease of conflict-driven changes in conscious experience.

Our results indicate that, by engaging in iterative and reciprocal interactions with sensory brain regions, inferior frontal cortex plays a critical role in both the detection and the resolution of perceptual conflicts. This points to a causal influence of prefrontal brain activity on the dynamic unfolding of conscious experience.

3 One-sentence Summary

Inferior frontal cortex detects and resolves perceptual conflict during bistable perception.

4 Introduction

The neural basis of conscious experience is one of today's greatest mysteries[1]. Its unravelling will have important implications for how we approach patients who remain unresponsive after brain damage or who suffer from hallucinatory distortions of perception[2]. Likewise, such progress may expand our ability to detect the presence of conscious experience in organic and artificial life beyond the human mind[3]. Yet, solutions to these problems remain elusive, since they require identifying not only the *neuro-anatomic correlates* of consciousness[4], but also the *computational function* of specific brain regions for conscious experience[5].

In the search for such a neuro-computational understanding of consciousness, the role of prefrontal brain areas is currently one of the most debated topics[6,7]. While some theories have ascribed a critical role to the prefrontal brain in generating perceptual consciousness[6,8–10], others have allocated the neuro-anatomy of conscious experience to more posterior brain regions[4,7,11]. The latter accounts link prefrontal activity to cognitive processes that occur in the wake of conscious experience[12,13], such as evaluating or acting on the contents of perception[14].

Bistable perception has been a key experimental approach in this debate for more than two decades[15]. In this phenomenon, stimuli that are compatible with two interpretations give rise to *perceptual conflict*[16]. Faced with this conflict, observers perceive periodic changes in conscious experience, oscillating between two mutually exclusive perceptual states[17]. Thereby, bistable perception provides a unique window into a fundamental neuro-computational aspect of consciousness: the transformation of ambiguous sensory information into unambiguous conscious experience[18–20].

Functional neuroimaging studies in humans have identified the right inferior frontal cortex (IFC; a subregion of prefrontal cortex, Figure 1A) as a key region in bistable perception[15]: When compared to stimulus-driven changes in perception, spontaneous perceptual changes during bistability were consistently found to be associated with increased activity in IFC[15].

This observation has been suggested to indicate that prefrontal cortex actively contributes to conscious experience[17,19,21–23]. According to this account, IFC may have a key role in resolving perceptual conflict by triggering perceptual changes through feedback signaling to sensory areas[17,19] (Figure 1A).

However, this *feedback*-account has been questioned by work that related IFC activity to the quality[25,26], report[27] and reportability[28,29] of changes in conscious experience during bistable perception. Perceptual conflict may thus rather be resolved within visual cortex and elicit activity in IFC through a *feedforward* mechanism. Accordingly, IFC activity may not reflect the cause, but the consequence of changes in conscious experience.

To settle the ongoing controversy between these feedforward- and feedback-accounts of bistable perception will be a critical step in elucidating the role of prefrontal cortex in consciousness. Here, we conjectured that these seemingly contradictory views may be reconciled within one computational characterization of IFC that incorporates both feedforward and feedback processing.

Firstly, we hypothesized that IFC may signal perceptual conflicts that arise between the contents of conscious experience and the available sensory data through a feedforward mechanism. To empirically test this hypothesis, we used functional magnetic resonance imaging (fMRI) in conjunction with computational modeling in a Bayesian framework. Secondly, we reasoned that the detection of perceptual conflict by IFC may in turn trigger changes in conscious experience via feedback signaling to sensory areas. This latter hypothesis was tested by disrupting IFC activity through neuronavigated transcranial magnetic stimulation (TMS).

5 Results

In a series of three experiments (E1-E3, Supplementary Figure S1), human observers reported changes in their perception of a rotating sphere (rightward-, leftward or unclear direction of rotation). In this *structure-from-motion* stimulus, random dots distributed on two intersecting rings induce illusory 3D motion (see Supplementary Video 1 and Supplementary Materials 10.1). Due to the perceptual conflict inherent in the ambiguous visual input, participants perceived spontaneous changes between left- and rightward rotation, which occurred every 25.08 ± 2.57 sec (*phase duration*, i.e., the average time spent between two consecutive changes in conscious experience; Supplementary Figure S2A-B).

Importantly, with this type of stimulus, changes in perceived direction of rotation occur only when fore- and background of the illusory sphere overlap[24,30] (Supplementary Figure S3A-B). This perceptual feature was pertinent to our approach in two ways: In addition to increasing the temporal precision of our analyses, it allowed us to compute response times (average $RT = 0.81 \pm 0.05$ sec) as an implicit measure of processes associated with behavioral reports[27,28].

5.1 IFC detects accumulating perceptual conflict

Bayesian perceptual inference[31] provides a plausible computational explanation for the effects of conflicting stimulus information on perception. In this framework, conscious experience is understood as an iterative process, constantly generating and testing *hypotheses* about the most likely cause of sensory data[32–35]. In bistable perception, the two alternating stimulus interpretations reflect mutually exclusive hypotheses that are both compatible with, but cannot fully account for the ambiguous sensory data. This results in perceptual conflict[22].

As a quantitative representation of such perceptual conflict, the residual evidence for the alternative to the currently dominant stimulus interpretation can be conceived of as a *perceptual prediction error*[20]. This unexplained error induces a progressive shift in the balance between the two perceptual hypotheses[23]. Over time, prediction errors thus accumulate until

the increasing perceptual conflict is reduced by a change in conscious experience from the dominant to the alternative stimulus interpretation (Figure 1B). A recent proof-of-concept study has linked this process to neural activity in prefrontal cortex[23]: During ambiguous visual stimulation, BOLD signals in IFC gradually increased while perception remained constant, peaking at the time of a conflict-induced change in conscious experience.

In experiment E1 (Supplementary Figure S1A), we sought to (1) confirm the previously suggested role of IFC in detecting perceptual conflict and to (2) test the hypothesis that such perceptual conflict originates from visual cortex.

To identify the neural representation of perceptual conflict, we acquired fMRI data during bistable perception and searched for correlations of BOLD activity with the dynamics of perceptual prediction errors. To this end, we inverted an established computational model of bistable perception[20,23] (see Supplementary Materials 10.2) based on the individual participants' behavioral reports on perceptual changes. This model estimates dynamic perceptual prediction errors to explain the sequence of conscious experiences during bistable perception. In model-based fMRI, we searched for the neural correlates of the estimated perceptual prediction errors while controlling for BOLD activity associated with the timing and report of perceptual changes. In line with previous results[23], we found that perceptual prediction errors were strongly reflected by BOLD activity in right-hemispheric IFC (anterior insula, inferior frontal gyrus[15]; Bonferroni-corrected for family-wise error $p_{FWE} < 0.05$, Figure 1C, Table 1).

This association with perceptual prediction errors suggests that IFC activity gradually accumulates while perception remains constant and peaks at the time of changes in conscious experience, by which IFC activity is, in turn, reduced[23] (see Figure 1B). Of note, previous studies have predominantly linked IFC to event-related processes associated specifically with perceptual changes[15]. We reasoned that this often-reported finding of change-related activity in IFC may actually correspond to the peak of accumulating prediction errors.

In our data, we could indeed only detect IFC-activity associated with changes in conscious experience if the analysis did not control for the correlation of BOLD signals with accumulating perceptual prediction errors (Supplementary Figures S4A and S4B, Table 1). In a direct comparison, we contrasted the explanatory power of perceptual prediction errors against a change-related regressor using posterior probability maps[36]. Crucially, BOLD activity in right-hemispheric IFC was better explained by prediction errors that gradually accumulated in each perceptual phase than by events associated with perceptual changes (exceedance probability $> 95\%$, Supplementary Figure S5).

During bistable perception, neural signals in IFC thus reflected the gradual accumulation of perceptual conflict and its reduction at the time of conflict-driven changes in conscious experience (see below for a replication of this finding in experiment E2). Yet, as a supra-modal brain region, IFC is unlikely to represent visual information independently of sensory brain regions. We therefore hypothesized that signals of perceptual conflict may be fed forward to IFC from the representation of perceptual content in visual cortex[37].

Indeed, perceptual conflict was additionally represented in the motion-sensitive extrastriate visual area V5/hMT+[38,39] (Figure 1C and Supplementary Figure S5). In contrast to IFC, neural activity in V5/hMT+ also predicted the content of conscious experience, that is, whether participants experienced leftward or rightward rotation during bistable perception: Based on multi-voxel pattern analysis[40] of BOLD signals in V5/hMT+, we were able to decode which of the two stimulus interpretations was, at a given point in time, *dominant* or *suppressed* (Supplementary Materials 10.3 and Supplementary Figure S6).

We therefore asked whether the neural correlates of perceptual conflict originated from the representation of the currently suppressed stimulus interpretation in V5/hMT+. To this end, we delineated V5/hMT+ based on the effects of visual stimulation (i.e., independently of our computational model of bistable perception). Within V5/hMT+, we identified *biased* voxel populations that showed elevated neural activity during either leftward (L) or rightward (R)

illusory rotation (T-value > 1; average number of voxels per population = 33.97 ± 1.78). While controlling for effects related to perceptual changes, we tested how BOLD activity in *L*- and *R-voxels* correlated with perceptual prediction errors.

Indeed, signals of perceptual conflicts emanated from neuronal populations in visual cortex that code for the currently suppressed stimulus interpretation: BOLD activity in L-voxels, that is, voxels that showed enhanced activity during perception of leftward rotation, correlated more strongly with perceptual prediction errors when participants perceived rightward rotation (paired t-test: T(32) = -5.26, p = 9.22×10^{-6}, $BF_{10} = 2.24 \times 10^{3}$, Figure 3A). Conversely, activity in R-voxels correlated more strongly with perceptual prediction errors when the participants consciously perceived leftward rotation (T(32) = 5.32, p = 7.94×10^{-6}, $BF_{10} = 2.57 \times 10^{3}$; see below for a replication of this finding in E2). Importantly, the dissociation between the representation of perceptual content and perceptual conflict depended on the strength of voxel biases (Supplementary Figure S7A).

5.2 IFC is sensitive to graded changes in perceptual conflict

The results of E1 suggested that IFC receives feedforward information about perceptual conflict, originating from the representations of ambiguous stimuli in visual cortex. Yet, in everyday perception, the fully ambiguous stimuli that give rise to bistable perception are rare[41]. Rather, perceptual processing usually occurs in the light of additional (i.e., *disambiguating*) stimulus information[42]. In experiment E2, we sought to confirm the role IFC in the signaling of perceptual conflict by measuring its responses to such disambiguating stimulus information. Thereby, we extended our computational account of prefrontal cortex beyond the special case of full sensory ambiguity.

To this end, we conducted an independent fMRI-experiment (Supplementary Figure S1B) based on *graded ambiguity*[43]. This novel paradigm modulates the strength of perceptual conflict by introducing varying degrees of disambiguating stimulus information for one over

the other percept (i.e., parametric 3D signals[39] that manipulate the *signal-to-ambiguity ratio* of the structure-from-motion stimulus). If an observer adopts a percept that is *congruent* with such disambiguating stimulus information, perceptual conflict is reduced. Accordingly, conflict-driven changes in conscious experience toward the alternative stimulus interpretation become less likely (Figure 1B, lower panel). Conversely, if the observer adopts a percept that is *incongruent* with the disambiguating stimulus information, perceptual conflict is enhanced. As a consequence, conflict-driven changes in conscious experience toward the alternative stimulus interpretation become more likely. Based on our hypothesis that IFC detects perceptual conflict, we predicted that IFC activity should be enhanced during incongruent as compared to congruent perceptual states. Furthermore, this enhancement should increase at higher signal-to-ambiguity ratios.

In analogy to E1, participants in E2 reported changes in the perceived direction of rotation of a structure-from-motion stimulus (rightward-, leftward or unclear direction of rotation). In runs with graded ambiguity, we introduced random changes in the direction of additional disambiguating 3D information. The frequency of these stimulus changes was informed by the individual participants' frequency of perceptual events experienced during full ambiguity. By attaching the disambiguating 3D signal to a fraction of the stimulus dots, we varied the signal-to-ambiguity ratio across six levels (D1 to D6).

As previously reported[43], the additional 3D signals biased conscious experience toward perceptual states that were congruent with the disambiguating stimulus information (T(19) $= 8.45$, p $= 7.37 \times 10^{-8}$, $BF_{10} = 1.97 \times 10^{5}$; Figure 4A). Crucially, for increasing signal-to-ambiguity ratios, congruent perceptual states were indeed more frequent (F(95) $= 51.14$, p $= 1.84 \times 10^{-25}$, $BF_{10} = 2.88 \times 10^{22}$).

Next, we assessed how the modulation of conscious experience by disambiguating stimulus information related to perceptual conflict. To this end, we inverted the computational model of bistable perception (see above and Supplementary Materials 10.2) based on the participants'

behavioral reports. As a quantitative representation of perceptual conflict, we compared average prediction errors according to the factors *Congruency* (incongruent vs. congruent perceptual states) and *Signal-to-Ambiguity* (D1-D6).

In line with our hypothesis, prediction errors were elevated during incongruent as compared to congruent perceptual states (main effect of *Congruency*: F(209) = 158.08, p = 2.29×10^{-27}, $BF_{10} = 3.06 \times 10^{20}$, Figure 4B). This effect increased with higher signal-to-ambiguity ratios (interaction between *Congruency* and *Signal-to-Ambiguity*: F(209) = 10.41, p = 6.19×10^{-9}, $BF_{10} = 2.57 \times 10^{6}$). During graded ambiguity, perceptual conflict (as reflected by perceptual prediction errors) was thus modulated by the signal-to-ambiguity ratio of visual stimulation (see Supplementary Figure S8 for a simulation of this effect).

Next, we asked whether this pattern was reflected by neural activity in IFC and V5/hMT+. To this end, we analyzed fMRI data recorded during graded ambiguity by comparing incongruent to congruent perceptual states separately for all levels of signal-to-ambiguity ratio. Again, we controlled for variations in BOLD signals associated with reported changes in conscious experience. This approach, which was independent of the assumptions inherent in our computational model of bistable perception, revealed enhanced BOLD signals during incongruent perceptual states in right-hemispheric IFC and V5/hMT+ (main effect of *Congruency*, $p_{FWE} < 0.05$, Figure 1D; see Table 2 for additional activations). As predicted, both right-hemispheric IFC and V5/hMT+ showed larger differences between incongruent and congruent perceptual states at higher signal-to-ambiguity ratios (interaction between *Congruency* and *Signal-to-Ambiguity*, small-volume correction at $p_{SVC} < 0.05$ within the main effect of *Congruency*).

These standard fMRI analyses were corroborated by model-based fMRI, which provided a complete replication of E1: While controlling for change-related activity, we again found that accumulating perceptual prediction errors correlated with neural activity in right-hemispheric IFC and V5/hMT+ ($p_{FWE} < 0.05$, Figure 1C and Table 1). In comparison to the analysis

based on perceptual change events, the dynamic accumulation of perceptual conflict was better at explaining BOLD signals in right-hemispheric IFC (exceedance probability > 95%, Supplementary Figure S5). Again, we found that the neural representation of perceptual conflict by L- and R- voxels in V5/hMT+ (average number of voxels per population = 32.92 ± 3.12) dissociated from the representation of current conscious experience (Supplementary Figure S6): BOLD activity in L-voxels correlated more strongly with accumulating perceptual prediction errors when participants perceived rightward rotation (paired t-test: T(19) = -4.07, p = 6.49×10^{-4}, BF_{10} = 53.36) and vice versa (T(19) = 3.11, p = 5.71×10^{-3}, BF_{10} = 8.2, Figure 2B and Supplementary Figure S7B).

In sum, both standard and model-based imaging results of E2 clearly show that IFC signals dynamic changes in perceptual conflict. To ascertain the specificity of these findings to perceptual conflict, we performed two additional control analyses (Supplementary Materials 10.4) that ruled out variations in perceptual uncertainty as well as temporal imbalances between congruent and incongruent perceptual states as alternative explanations for our fMRI results.

5.3 Disruption of neural activity in IFC modulates the dynamics of conscious experience

So far, converging evidence from two independent fMRI experiments strongly suggested that IFC detects the conflict inherent in sensory ambiguity. In a third experiment (E3), we asked whether this unconscious accumulation of perceptual conflict in IFC is relevant for conscious experience. To this end, we used inhibitory TMS with a theta-burst stimulation protocol[44] to create *virtual lesions* in IFC. We reasoned that, if changes in conscious experience during bistable perception were facilitated by the neural representation of perceptual conflict in IFC, its disruption by TMS should reduce the frequency of such conflict-driven changes in conscious experience during bistable perception.

In E3, we re-invited the participants from E1 for two TMS sessions scheduled on consecutive days. In each session, they first reported changes in conscious experience during two runs of ambiguous structure-from-motion. This was followed by 40 sec of TMS to either IFC or a control location at the cranial vertex (order counter-balanced across participants). Immediately afterwards, participants again reported their perception during two runs of ambiguous structure-from-motion.

To ensure spatial precision, we delivered TMS using fMRI-informed neuronavigation. We delineated individual IFC stimulation sites based on BOLD activity associated with perceptual changes in E1 (MNI = [55.6 $\pm$ 0.4 15.5 $\pm$ 0.39 10 $\pm$ 0.49]). By informing the TMS-intervention based on the conventional change-related approach to IFC[24,26,28], we delineated the IFC stimulation site independently of our computational model of bistable perception[23]. As shown above, change-related activity coincided with the neuro-anatomic correlates of perceptual prediction errors (Figure 1C, Supplementary Figure S4B), which had more explanatory power with regard to BOLD signals in IFC[23] (Supplementary Figure S5). As expected, activity in the IFC stimulation site was thus highly correlated to perceptual prediction errors (average regression coefficients in spherical ROIs of 10 mm radius around individual coordinates: β = 1.79 $\pm$ 0.38; T(32) = 4.75, p = 4.15×10^{-5}, BF_{10} = 565.3).

The control stimulation site at vertex was determined by anatomical (T1) scans (MNI = [0 -25 85]). Given the spatial resolution of neuronavigated TMS[45], vertex-TMS was extremely unlikely to exert local effects on any additional neural correlates of bistable perception (Table 1).

After neural activity in IFC was disrupted by TMS, changes in conscious experience occurred less frequently: For virtual lesions in IFC, we observed prolonged perceptual phase durations (post-pre: 6.86 $\pm$ 1.79 sec) relative to the vertex condition (-1.59 ± 2.07 sec; paired t-test: T(29) = -3.44, p = 1.77×10^{-3}, BF_{10} = 20.05; Figure 4A). This finding strongly suggests that IFC not only detects gradually accumulating perceptual conflict, but also has a causal

role in triggering changes in conscious experience.

Two additional control analyses addressed alternative accounts of the observed TMS effect on perceptual phase durations. Firstly, previous work has shown that activity in frontal brain regions is elevated at the time of unclear perceptual states during bistability[26]. Here, however, disruption of neural activity in IFC did not alter frequency of unclear perceptual states (post-pre: $0.07 \pm 0.18\%$) in comparison to vertex-stimulation ($-0.26 \pm 0.26\%$; paired t-test: T(29) = -1.04, p = 0.31, $BF_{10} = 0.32$; Figure 4B).

Secondly, when investigating frontal activity as a potential driver of changes in conscious experience during bistable perception, reporting behavior represents a possible confound[14]. "No-report"-paradigms have elegantly addressed this issue, suggesting that a subset of change-related activations in prefrontal cortex may represent the neural correlates of reporting rather than consciousness[27]. Here, we used RTs to ask whether inhibition of activity in IFC impaired the participants' ability to report on the contents of conscious experience. Changes in RTs did not differ between IFC- (post-pre: $2.55 \times 10^{-3} \pm 0.01$ sec) and vertex-stimulation (0.02 ± 0.01 sec; paired t-test: T(29) = 0.77, p = 0.45, $BF_{10} = 0.26$; Figure 4C). In Supplementary Materials 10.5-7, we replicate these findings in linear mixed effects modeling (10.5) and rule out exposure effects (10.6) as well as regression toward the mean (10.7) as additional alternative explanations of our results.

In sum, disruption of activity in IFC reduced the frequency of changes in conscious experience during bistable perception. Importantly, we found no evidence for TMS effects on perceptual uncertainty or reporting behavior. These results thus support the hypothesis that IFC responds to conflicting sensory data by facilitating spontaneous changes in conscious experience, thereby temporarily resolving perceptual conflict[20,22,23].

5.4 Individual differences in the representation of perceptual conflict predict the effect of virtual IFC-lesions on conscious experience

Finally, we asked whether inter-individual differences in the effect of virtual IFC-lesions on bistable perception (E3) could be predicted by the fMRI-data acquired prior to the TMS-intervention (E1). We reasoned that virtual IFC-lesions should suppress conflict-induced changes of conscious experience to a greater extent in participants who showed a stronger representation of perceptual conflict in IFC (as expressed by the individual regression coefficient β of perceptual prediction errors to BOLD signals in IFC stimulation sites).

Indeed, we confirmed that the representation of perceptual prediction errors in IFC predicted the effect of virtual IFC-lesions on conscious experience ($\rho = 0.42$, $p = 0.02$, Figure 4D). In contrast, we observed no correlation with differences in phase duration after TMS to vertex ($\rho = 0.11$, $p = 0.58$). Moreover, the representation of perceptual prediction errors in IFC was uncorrelated to inter-individual differences in perceptual uncertainty ($\rho = 0.02$, $p = 0.91$) and RTs ($\rho =$ -0.08, $p = 0.69$) observed in association with virtual lesions in IFC.

This result provides a direct link between the neural representation of perceptual conflict in IFC and the effect of virtual lesions on conscious experience. Our findings therefore strongly suggest that the detection of perceptual conflict by IFC is tightly coupled to its active role in the resolution of such conflict.

6 Discussion

In this work, we found compelling evidence for a pivotal role of IFC in conscious experience. Two independent fMRI experiments demonstrated that IFC signals the accumulating conflict between conscious experience and the underlying sensory data. Crucially, TMS-induced virtual lesions revealed that IFC facilitates changes in conscious experience that occur in response to perceptual conflict. Together, these findings reconcile the feedforward- and feedback-accounts of bistable perception, suggesting a hybrid computational function of IFC: the detection and resolution of perceptual conflict.

By involving hierarchical inference in the resolution of sensory ambiguity, our results may seem to contradict the well-established dynamic system account of bistable perception[46,47]. This framework proposes that, in the context of conflicting stimulus information, changes in conscious experience emerge from local mechanisms such as inhibition[48], adaption[49,50] or noise[51] in sensory brain regions. Yet, the *implementational* concept of local adaption-and-inhibition[46,47] and the *algorithmical* hypothesis of hierarchical conflict-accumulation[20,23] are by no means mutually exclusive, but seem likely to represent two sides of the same coin[15]. Our current results provide empirical evidence for this complementarity: In visual cortex, perceptual conflict was predominantly represented by voxels that code for the currently suppressed stimulation interpretation. Prior to changes in conscious experience, BOLD signals thus progressively increase in the neural representation of conflicting stimulus information. This may be tantamount to a gradual escape from inhibition, as adaption reduces neural activity in the voxels dominating the current content of conscious experience.

Possibly, the capacity of IFC to detect perceptual conflict may be limited to situations in which the competing states are perceptually distinguishable. When they are not[29], IFC may fail to read out conflicting stimulus representations[37,52], leaving the resolution of perceptual conflict to sensory brain regions[53]. This may provide a plausible explanation for the absence of frontal activations when perceptual events are invisible[28]. Likewise, our results provide a

parsimonious account of enhanced neural activity observed during unclear or *mixed* conscious experience[26], since such perceptual states may represent instances of enhanced perceptual conflict.

With respect to the role of prefrontal cortex in consciousness, our results clearly speak against the notion that IFC activates merely as a consequence of perceptual events that are generated within sensory cortices[26–28]. In line with recent electrophysiological data in monkeys[54], our findings strengthen existing theoretical accounts[6,8–10] that assume a critical role of prefrontal cortex in consciousness. As a significant extension, our work associates IFC with a specific computational function for conscious experience: In iterative feedback- and feedforward-interactions with sensory brain regions, IFC may determine how swiftly conscious experience is updated in response to perceptual conflict[19,20,23]. Thereby, IFC may ensure that perception is altered when discrepancies between conscious experience and sensory data have accumulated over time, but remains stable when perceptual conflicts are transient.

Such an adaptive function in the response to perceptual conflict connects IFC to the *homeostasis*[55] of consciousness. Beyond the context of gating conflicting sensory information into conscious experience, IFC may be play a similar homeostatic role in orienting toward relevant stimuli[56], in detecting change[57,58], in allocating object-based attention[52] or in exerting cognitive control[59,60]. This multitude of adaptive functions argues for a fundamental impact of prefrontal brain activity on conscious experience: In a world that is cloaked by noise and ambiguity, IFC may participate in a hierarchy of predictive processes[61] that enable perceptual systems to leverage prior knowledge when inferring on the most likely cause of sensory information[32–35].

Altered states of consciousness such as hallucinations[62,63] could therefore relate directly to an impaired homeostatic processing of sensory information in IFC. Previous research has associated sensitivity to perceptual conflict with the severity of hallucinations[43]. Correspondingly, functional imaging has repeatedly linked hallucinations to neural activity in IFC[64,65].

In focusing predominantly on temporoparietal cortex, TMS-protocols have yielded mixed results in the treatment of hallucinations[66]. Non-invasive brain stimulation of IFC may thus represent a promising new approach in the search for the neural basis of altered states of consciousness.

7 Methods and Materials

7.1 Participants

Experiment E1 consisted of a behavioral pre-test (Runs 1 and 2) and an fMRI-experiment (Runs 3 - 5). We recruited a total of 35 participants. Based on the behavioral pre-test, we excluded two participants who performed at chance-level when discriminating the direction of rotation of a fully disambiguated structure-from-motion stimulus. Thus, 33 participants took part in the fMRI-experiment (21 female, mean age: 27.3 ± 1.42 years). All participants agreed to be contacted later for a follow-up experiment using TMS (E3, see below).

Experiment E2 consisted of a behavioral pre-test and a fMRI-experiment. We recruited a total of 23 participants. We excluded three participants who performed at chance-level when discriminating the direction of rotation of a fully disambiguated structure-from-motion stimulus. The final sample thus consisted in 20 participants (11 female, mean age: 27.7 ± 0.98 years).

For experiment E3, we re-invited the participants from E1 to two TMS session scheduled on consecutive days. From this group, one participant could not be re-contacted at the time of the TMS-experiment. Two further participants did not tolerate the TMS-procedure. The final TMS-sample thus consisted of 30 participants (19 female, mean age: 27.33 ± 1.56 years).

All participants were right-handed, showed corrected-to-normal vision, had no prior neurological or psychiatric medical history and gave written informed consent prior to taking part in the study. All procedures were approved by the ethics committee at Charité Berlin.

7.2 Stimuli

Stimuli were presented using Psychtoolbox 3[67] and Matlab R2007b (behavioral pre-test: CRT-Monitor at 60 Hz, 1042 x 768 pixels, 60 cm viewing distance and 30.28 pixels per degree visual angle; fMRI: LCD-Monitor at 60 Hz, 1280 x 1024 pixels, 160 cm viewing distance and

90.96 pixel per degree visual angle; TMS: LCD-Monitor at 60 Hz, 1280 x 1024 pixels, 60 cm viewing distance and 37.82 pixels per degree visual angle).

7.2.1 Random dot kinematograms

Throughout E1, E2 am E3, participants indicated their perception of a discontinuous random-dot kinematogram (RDK, see Video 1). In this stimulus, random dots distributed on two intersecting rings induce the perception of a spherical object rotating either left- or rightward around a vertical axis[30] (diameter: 15.86°, rotational speed: 12 sec per rotation, rotations per block: 10, individual dot size: 0.12°). Each run consisted of six blocks of visual stimulation (120 sec), separated by fixation intervals (behavioral pre-tests: 5 sec; fMRI- and TMS-experiments: 10 sec).

Depending on the experimental condition (see Supplementary Figure S1), the RDK could appear in three configurations: Complete ambiguity, levels of graded ambiguity and complete disambiguation. Complete ambiguity was achieved by presenting identical stimuli to the two eyes. This induced periodic changes in conscious experience (also dubbed *endogenous transitions*) between left- and rightward rotation (i.e., bistable perception). For complete disambiguation, we used red-blue filter glasses (left eye: red channel, right eye: blue channel) to attach a stereo-disparity signal (1.8° visual angle) to all dots on the stimulus surface. By inverting the direction of rotation, we created stimulus-driven or *exogenous* changes in conscious experience. During graded ambiguity[43], we varied the proportion of disambiguated stimulus dots between 15%, 30%, 45%, 60%, 75% and 100% (conditions D1 to D6). This variation in the signal-to-ambiguity ratio parametrically modulated the perceptual conflict between conscious experience and visual stimulation. For graded ambiguity, we determined the individual frequency of exogenous stimulus changes based on the frequency of conflict-induced changes in conscious experience during full ambiguity.

We based our behavioral analyses on perceptual events as reported by the participants (right index-finger: rotation of the front-surface to the left; right ring-finger: rotation to the right;

right middle-finger: unclear direction of rotation). Since the RDK is not depth-symmetric over all rotational angles[30], changes in conscious experience occurred only at overlapping configuration of the stimulus (see Supplementary Figure S2A-B). We thus corrected the timing of perceptual events to the last overlapping configuration of the stimulus preceding the button-press, representing the perceptual time-course as a discrete sequence of perceptual states (rotation of the front-surface to the right/left and unclear direction of rotation).

To describe the temporal dynamics of bistable perception, we computed *average phase durations* (the time spent between two changes in conscious experience, i.e., multiples of the 1.5 sec inter-overlap-interval). The content of conscious experience was reflected by the dependent variables *directed bias* (the percentage of rightward perceptual states relative to the total number of perceptual states), *absolute bias* (the absolute difference between the absolute bias and chance level at 50%) and the percentage of *uncertain states*. To characterize processes involved in the behavioral report of perception, we computed *response times* by subtracting the timing of the last preceding overlapping configuration from the timing of the behavioral responses indicating a perceptual event. The impact of sensory data on perception was depicted by the dependent variable *perceptual congruency* (percentage of perceptual states congruent with the disambiguating 3D signal).

7.2.2 Heterochromatic flicker photometry

When using filter glasses (Experiment E2), the perceived direction rotation of RDKs can be biased by differences in the subjective luminance between red and blue (Pulfrich effect[68]). To estimate subjective equiluminance, we presented red and blue circles (diameter: 6.45°) alternating at a frequency of 15 Hz. Differences in subjective luminance of red and blue stimuli led to the experience of flicker. Participants reduced the flicker by adjusting the luminance of the red stimulus initially presented at a random luminance between 0% and 255% relative to the blue stimulus presented at a fixed luminance. Average equiluminance estimated across 10 such trials determined the monitor- and participant-specific luminance of

the red- and blue-channels (average blue-channel luminance relative to red-channel: 2.02 ± 0.09).

7.2.3 2D control stimuli

At higher levels of signal-to-ambiguity, perceptual states were less likely to be incongruent with the disambiguating stimulus information. Hence, increments in the signal-to-ambiguity ratio increased the temporal imbalance between congruent and incongruent perceptual states. To test for potential confounds introduced by temporal imbalance, we constructed a 2D control version (E2, Run 8) of the bistable RDK (identical stimulus diameter, number, size and speed of dots). Participants reported the direction of planar, horizontal 2D motion. For each participant, changes in the direction of planar dot motion were determined by both the temporal imbalance between congruent and incongruent perceptual phases (separately for conditions D1-D6) as well as the average frequency of changes in conscious experience observed in the main experiment (E2, Runs 5-7). We randomized the motion direction associated with reduced presentation-time.

7.3 FMRI

7.3.1 Acquisition and preprocessing

For E1 and E2, we recorded a T1-weighted MPRAGE sequence (voxel size 1 x 1 x 1 mm) for anatomical images and used T2-weighted gradient-echo planar imaging (TR 2000 ms, TE 25 ms, voxel-size 3 x 3 x 3 mm) to obtain a total of 400 BOLD images per run on a Siemens Prisma 3-Tesla-MRI-system (64-channel coil). Our pre-processing routine was carried out within SPM12 and consisted in slice time correction with reference to the middle slice, standard realignment, coregistration and normalization to MNI stereotactic space using unified segmentation. For standard analyses, we applied spatial smoothing with 8 mm full-width at a half-maximum isotropic Gaussian kernel. For the analysis of voxel biases and

decoding, we used unsmoothed data.

7.3.2 General linear models

To test for the neural correlates of perceptual conflict during sensory ambiguity in E1 and E2, we extracted dynamic perceptual prediction errors from the predictive-coding (PC) model of bistable perception[23], which was inverted based on behavioral data. This *model-based* fMRI approach (**GLM-PC**) defined visual stimulation by stick-regressors aligned to the overlapping configurations of the structure-from-motion stimulus (*overlaps*). Relative to the *overlaps*, we defined two parametric regressors ordered as follows: (1) perceptual *changes* (binary; 0: no change, 1: change) and (2) absolute *prediction errors* (continuous, ranging from 0 to 1). For the analysis of direction-specific effects in voxel biases within V5/hMT+, the overlaps and the associated parametric modulators were modeled separately according to the current perceptual state (left- vs- rightward rotation). In addition to standard GLMs, we performed Bayesian second-level statistics[36] to compare the explanatory power between change-related models and prediction-error related models with regard to BOLD activity in IFC. To this end, we deleted one of the two parametric modulators in GLM-PC, creating Log-Evidence-Maps for the two degraded models ("PE only" vs. "Change only"; z-scored parametric modulators).

In E2, we used an additional GLM (**GLM-Congruency**) to analyze BOLD activity during graded ambiguity independently of the assumptions inherent in the predictive-coding model of bistable perception. Next to perceptual changes (T, stick-function), this GLM represented perceptual states by box-car regressors defined according to two factors: Firstly, perceptual states could be congruent (*C1*) or incongruent (*C2*) to conscious experience. Secondly, visual stimulation varied across six levels of signal-to-ambiguity (*D1-D6*). The GLM's design matrix contained all combinations between the two factors ([C1D1 C1D2 (...) C1D6 C2D1 C2D2 (...) C2D6 T]). By analogy, we tested for a potential effect of temporal imbalances between congruent and incongruent perceptual phases in the fMRI control-experiment (run E2(8)).

GLM-Control defined prolonged (*A1*) and shortened (*A2*) perceptual phases separately for all levels of temporal imbalance (Levels *I1* to *I6*; design-matrix = [A1I1 A1I2 (...) A1I6 A2I1 A2I2 (...) A2I6 T]).

In E3, we identified individual IFC stimulation sites based on the fMRI data acquired in E1. To delineate IFC independently of the assumptions inherent in the predictive-coding model of bistable perception (see GLM-PC), we adopted the conventional change-related fMRI approach to IFC[24,26,28], representing endogenous perceptual changes as stick-functions and visual stimulation as a box-car regressor (**GLM-Changes**).

In all GLMs, we convolved the outlined regressors with the canonical hemodynamic response function (SPM12), added six rigid-body realignment parameters as nuisance covariates, applied high-pass filtering at 1/128 Hz and computed first-level one-sample t-tests against baseline. On the second-level, the resulting images were submitted to second-level one-sample t-tests (GLM-PC) or full factorial models (GLM-Congruency and GLM-Control). Second-level results were thresholded at $p < 0.05$ (FWE-corrected across the whole brain; SVC within orthogonal activation maps for GLM-Congruency). For Bayesian second-level statistics[36], we display second-level results at an exceedance probability of 95% for "PE only".

7.3.3 Stimulation-Sites in IFC and vertex

In E3, we defined individual IFC coordinates for neuronavigated TMS independently of the assumptions inherent in the predictive-coding model of bistable perception. Using GLM-Changes, we identified the peak voxel for "Changes vs. baseline" (first-level contrast at $p < 0.005$, uncorrected) within a literature-based IFC search-sphere (radius = 5 mm; centre = [57 17 10]). This location was motivated by the neural correlates of conflict-driven as opposed to stimulus-driven changes in conscious experience in a closely related structure-from-motion stimulus[23]. Across participants, average stimulation-sites were located at MNI = [55.6 ± 0.4 15.5 ± 0.39 10 ± 0.49] (Changes vs. baseline: T = 8.21 ± 0.51).

Vertex coordinates for TMS were defined anatomically (standardized coordinates = [0 -25 85]) based on T1 scans.

7.3.4 Regions-of-interest (ROI)

All ROIs were defined independently of our computational model of bistable perception[23] (see Supplementary Materials 10.2). With respect to IFC, we defined spherical ROIs (radius: 10 mm) around the individual IFC-TMS coordinates (see above). To delineate V5/hMT+, we constructed a search sphere (radius: 5 mm) around the peak-voxel for the second-level contrast "Visual Stimulation vs. baseline" (GLM-Changes, $p_{FWE} < 0.05$) within an anatomical mask for V5/hMT+[69]. Based on this search sphere, we constructed individual V5/hMT+-ROIs (radius: 10 mm) centered around the individual peak coordinates of the corresponding first-level contrast (p $<$ 0.005, uncorrected). Within these ROIs, we defined voxels with biases for righward- and leftward perceptual states (L- and R-population) by thresholding the contrasts for "left vs. rightward perceptual states" and vice versa at a T-value of 1 (GLM-PC). Functional ROI-based analyses were carried out in Marsbar (http://marsbar.sourceforge.net/).

7.4 TMS

In E3, we used TMS with a theta-burst protocol to induce virtual lesions in two stimulation sites (i.e., the target-region in right-hemispherical IFC and the control-region at the cranial vertex). TMS was delivered in two separate TMS-sessions on two consecutive days. We counterbalanced the order of IFC- vs vertex-TMS across participants. Participants performed two runs of the experiment prior to TMS and two runs immediately after TMS.

We delivered TMS with a focal, figure-of-eight-shaped coil equipped with active cooling. Pulses where generated using a standard MagPro R30 stimulator (MagVenture Ltd, Farum, Denmark). Stimulation was guided by neuro-navigation based on individual change-related BOLD activity in IFC projected onto the participants' T1 scans (data acquired during E1) using the Localite TMS Navigator (Localite GmbH, Bonn, Germany) with an optical tracking

camera PolarisVicra (Northern Digital Inc., Ontario, Canada). The coil was positioned tangentially to the subjects' head and adjusted such that the electric current in the center of the coil would run perpendicular to the course of the inferior frontal sulcus. Prior to each session, we identified individual resting motor thresholds (rMTs) for the right first dorsal musculus interosseous (FDI) by stimulation of left-hemispherical motor cortex[70]. The coil was held tangentially to the subject's skull at a 45° angle to the parasagittal line (4 cm lateral and 1 cm anterior to the vertex), and the search for the hot-spot was additionally guided through the optical tracking system in order to locate the hand-knob. In order to find the rMT hot-spot, we started with 55% Maximum Simulator Output (MSO) and increased the intensity in 5% steps. If a motor evoked potential (MEPs) was elicited, adjustments were made in 1% steps. Pulses for MT search were delivered with a minimum of 5 sec delay in order to avoid any change in excitability due to repeated stimulation. MEPs were recorded from the right FDI using self-adhesive gel electrodes in a standard belly-tendon fashion. RMTs were defined as the percentage of maximum stimulator output needed to evoke 50µV MEPs peak-to-peak in five out of ten consecutive trials (average rMT in vertex sessions: 41.67 ± 1.12% MSO; IFC sessions: 40.9 ± 1.15% MSO; paired t-test: $T(29) = 0.89$, $p = 0.38$, $BF_{10} = 0.28$). The theta-burst TMS-protocol consisted in a total 600 pulses applied within 40 sec (50-Hz bursts with three pulses applied in intervals of 200 ms) at an intensity of 80% rMT. Stimulation parameters were in line with published safety guidelines and were chosen to produce a decrease in cortical excitability[44,71–73] throughout the 25 min test-phase following TMS.

8 Figures

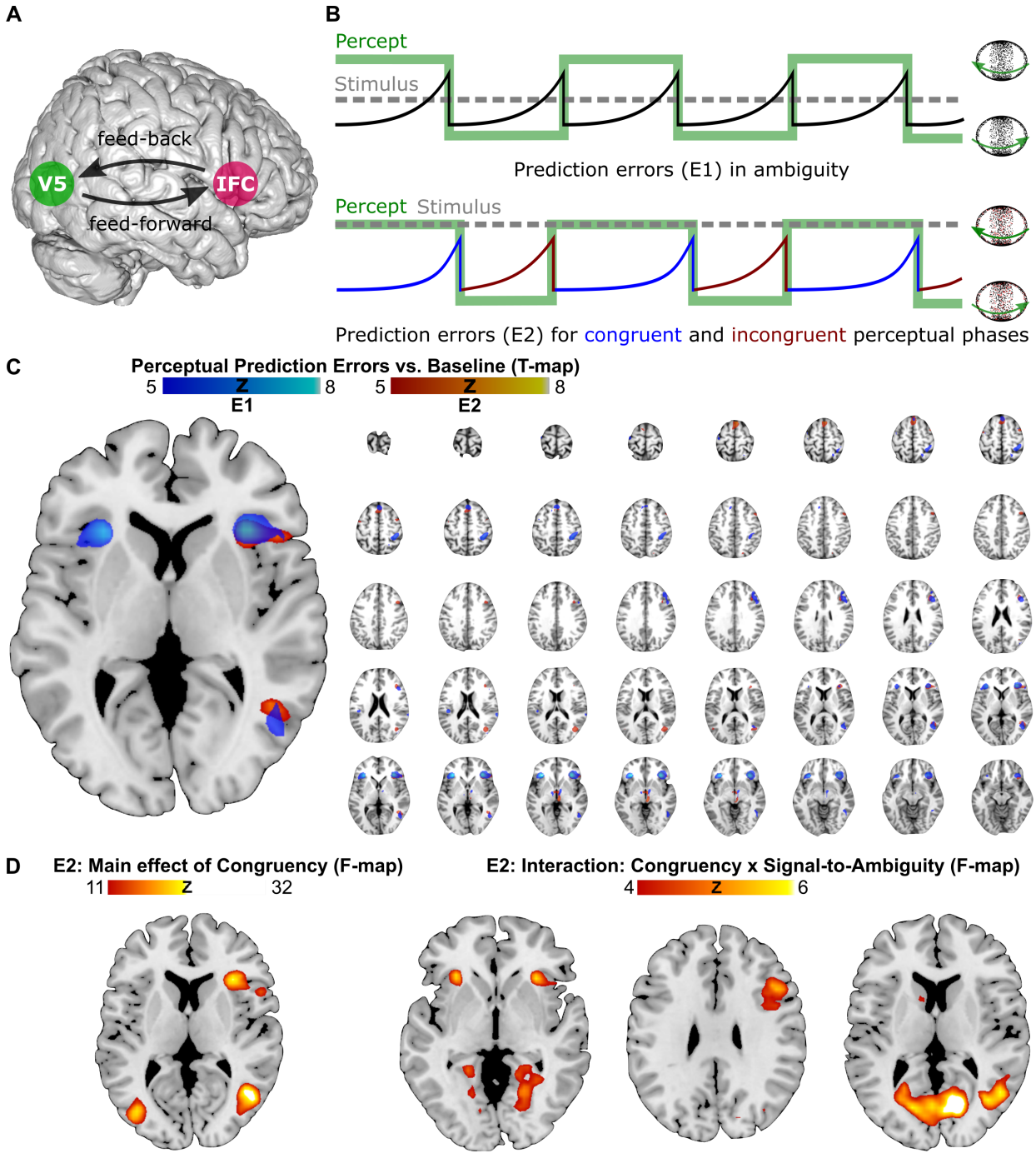

Figure 1. A. IFC in bistable perception. The role of IFC (schematic overlay in pink) in conscious experience is controversial: According to one view, feedback from IFC may modulate perceptual processing in visual cortex (motion-sensitive visual cortex V5/hMT+, highlighted in green). This may reflect an active contribution of prefrontal brain activity

to conscious experience. The opposing view links neural activity in IFC to the quality, report or reportability of perceptual events. This suggests that conscious experience may be realized within visual cortex and may drive activity in IFC by means of feedforward processing. **B. Accumulating perceptual conflict and conscious experience.** Here, we depict conscious experience and associated changes in accumulating perceptual conflict for bistable perception induced by a random dot structure-from-motion stimulus (RDK). The perceived direction of rotation (green line) of this bistable stimulus alternates between left- and rightward motion of the front-surface (icons on the right). As a quantitative representation of perceptual conflict, we display the dynamics of perceptual prediction errors. In the absence of disambiguating sensory evidence (upper panel; grey dotted line), the predictive-coding model of bistable perception (see Supplementary Materials 10.2) assumes accumulating prediction errors (black solid line) while perception remains constant, until perceptual conflict is reduced by a change in conscious experience. When additional stimulus information is introduced by graded ambiguity (lower panel; grey dotted line), perception fluctuates between perceptual phases congruent with current stimulus information (overlap between grey dotted line and green line) and perceptual phases incongruent with current stimulus information (divergence between grey dotted line and green line). During congruent perceptual phases, perceptual prediction errors are reduced and thus accumulate more slowly (blue solid line). In turn, incongruent perceptual phases are characterized by enhanced prediction errors, which accumulate more quickly (red solid line). Importantly, the signal-to-ambiguity ratio determines how strongly disambiguating stimulus information modulates perceptual prediction errors. **C. The neural correlates of accumlating perceptual conflict.** In model-based fMRI, we studied the relation of BOLD activity to accumulating perceptual prediction errors (E1: blue heatmap; E2: red heatmap). In line with previous results, both experiments yielded converging evidence that perceptual prediction errors correlated with neural activity in right-hemispherical IFC (including anterior insula and inferior frontal gyrus) and V5/hMT+. Additional activations were located in left insula,

right posterior-medial frontal gyrus and right inferior parietal lobulus (all $p_{FWE} < 0.05$, Table 1). **D. The neural correlates of graded ambiguity.** To assess the neural correlates of perceptual conflict independently of the assumptions inherent in our predictive-coding model of bistable perception, we analyzed the neural correlates of graded ambiguity according to the factors *Congruency* and *Signal-to-Ambiguity*. This approach represented congruent and incongruent perceptual states by box-car regressors, separately for all six levels of *Signal-to-Ambiguity*. We expected regions coding for perceptual conflict to show both a main effect of *Congruency* (enhanced BOLD signals during incongruent perceptual states) and an interaction between *Congruency* and *Signal-to-Ambiguity* (larger BOLD signal differences between congruent and incongruent perceptual states at higher levels of signal-to-ambiguity). In line with our predictions, we found a main effect of Congruency in right-hemispherical IFC (insula and inferior frontal gyrus) and V5/hMT+, alongside additional clusters in left precentral gyrus, right posterior-medial frontal gyrus (PMF) and right fusiform gyrus ($p_{FWE} < 0.05$). Importantly, right insula (left panel), inferior frontal gyrus (left and middle panel) and V5/hMT+ (right panel) also reflected a significant interaction between *Congruency* and *Signal-to-Ambiguity* ($p_{SCV} < 0.05$ within the main effect of *Congruency*), indicating that perceptual conflict was represented in these regions.

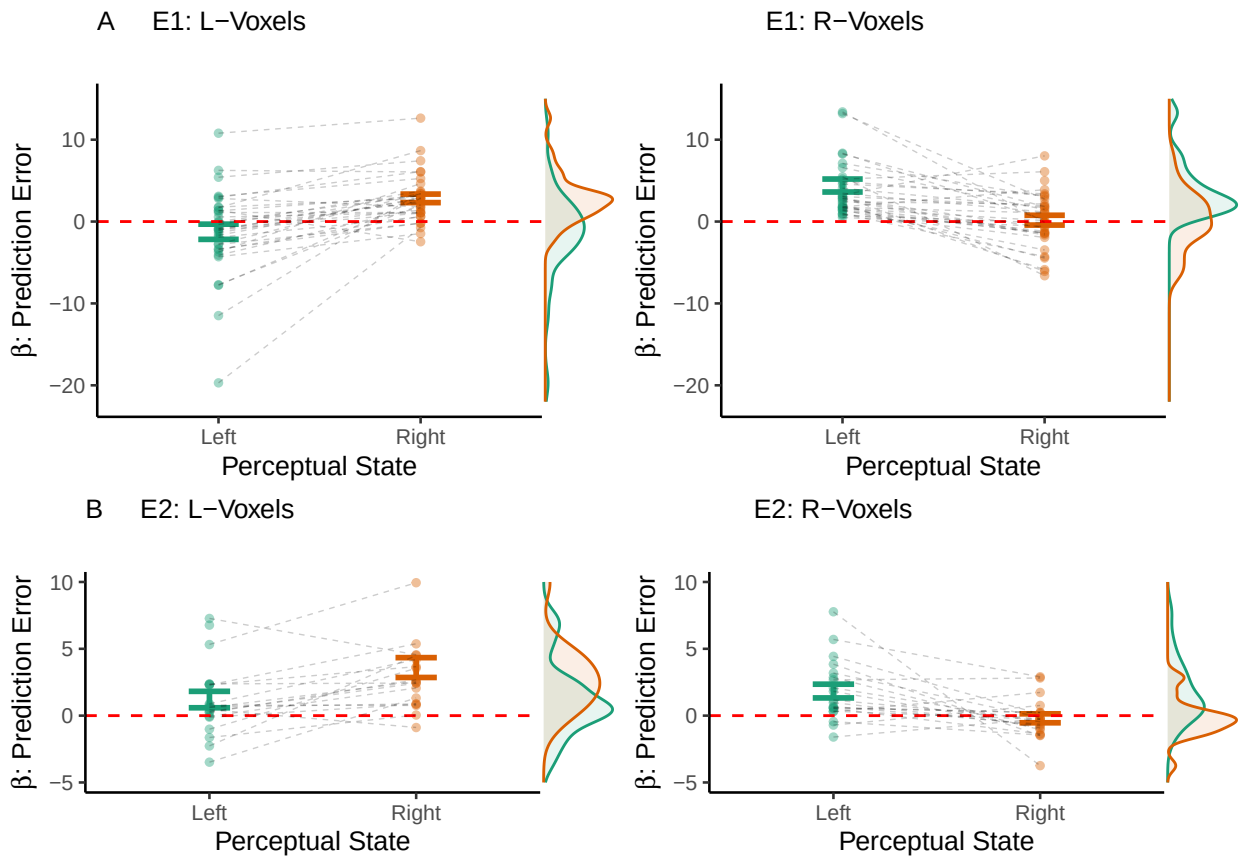

Figure 2. The neural correlates of perceptual conflict in V5/hMT+. A. Experiment E1. Here, we investigated whether the representation of perceptual conflict (i.e., the correlation to gradually accumulating perceptual prediction errors) depended on the current perceptual state. To this end, we delineated voxels with biases toward leftward (L) and rightward (R) rotation in V5/hMT+. The representation of perceptual states was dissociated from the representation of perceptual conflict: BOLD activity in L-voxels (left panel) was more strongly correlated with perceptual prediction errors when the participants consciously perceived rightward rotation (paired t-test: T(32) = -5.26, p = 9.22×10^{-6}, $BF_{10} = 2.24 \times 10^{3}$). In contrast, R-voxels (right panel) were more strongly correlated with perceptual prediction errors when the participants consciously perceived leftward rotation (T(32) = 5.32, p = 7.94×10^{-6}, $BF_{10} = 2.57 \times 10^{3}$). **B. Experiment E2.** Experiment E2 replicated these results: L-voxels (left panel) were more strongly correlated with perceptual prediction errors during illusory rotation toward the right (paired t-test: T(19) = -4.07,

p $= 6.49 \times 10^{-4}$, $BF_{10} = 53.36$). In turn, BOLD activity in R-voxels (right panel) was more strongly correlated with perceptual prediction errors when the participants consciously perceived leftward rotation (T(19) $= 3.11$, p $= 5.71 \times 10^{-3}$, $BF_{10} = 8.2$).

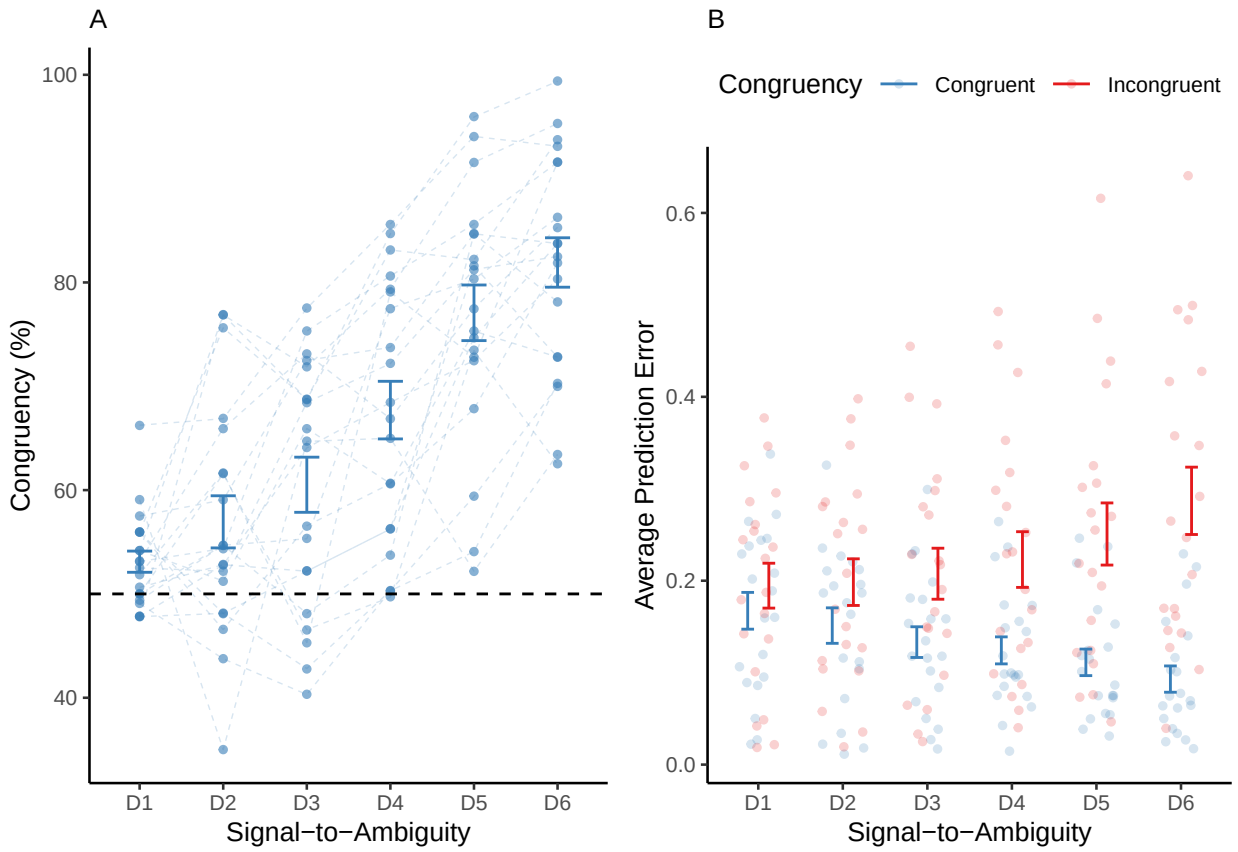

Figure 3. Perceptual conflict during graded ambiguity. A. Congruent perceptual states. In experiment E2, we presented additional disambiguating stimulus information at increasing signal-to-ambiguity ratios (D1-D6). Conscious experience was biased toward perceptual states that were congruent with the disambiguating stimulus information (T(19) = 8.45, p = 7.37×10^{-8}, $BF_{10} = 1.97 \times 10^{5}$). Importantly, the bias toward congruency was stronger for visual stimulation with high signal-to-ambiguity (F(95) = 51.14, p = 1.84×10^{-25}, $BF_{10} = 2.88 \times 10^{22}$). **B. Perceptual prediction errors during graded ambiguity.** To visualize the modulation of perceptual conflict during graded ambiguity, we estimated perceptual prediction errors using the predictive-coding model of bistable perception. We analyzed average prediction errors according to the factors *Congruency* (incongruent vs. congruent perceptual states) and *Signal-to-Ambiguity* (D1-D6). Prediction errors were elevated during incongruent as compared to congruent perceptual states (main effect of *Congruency*: F(209) = 158.08, p = 2.29×10^{-27}, $BF_{10} = 3.06 \times 10^{20}$). As expected,

the difference in prediction errors between congruent and incongruent perceptual states was enhanced for higher signal-to-ambiguity ratios (interaction between *Congruency* and *Signal-to-Ambiguity*: $\mathrm{F}(209) = 10.41$, $\mathrm{p} = 6.19 \times 10^{-9}$, $BF_{10} = 2.57 \times 10^{6}$). Overall prediction errors did not vary with *Signal-to-Ambiguity* ($\mathrm{F}(209) = 0.54$, $\mathrm{p} = 0.75$, $BF_{10} = 0.02$).

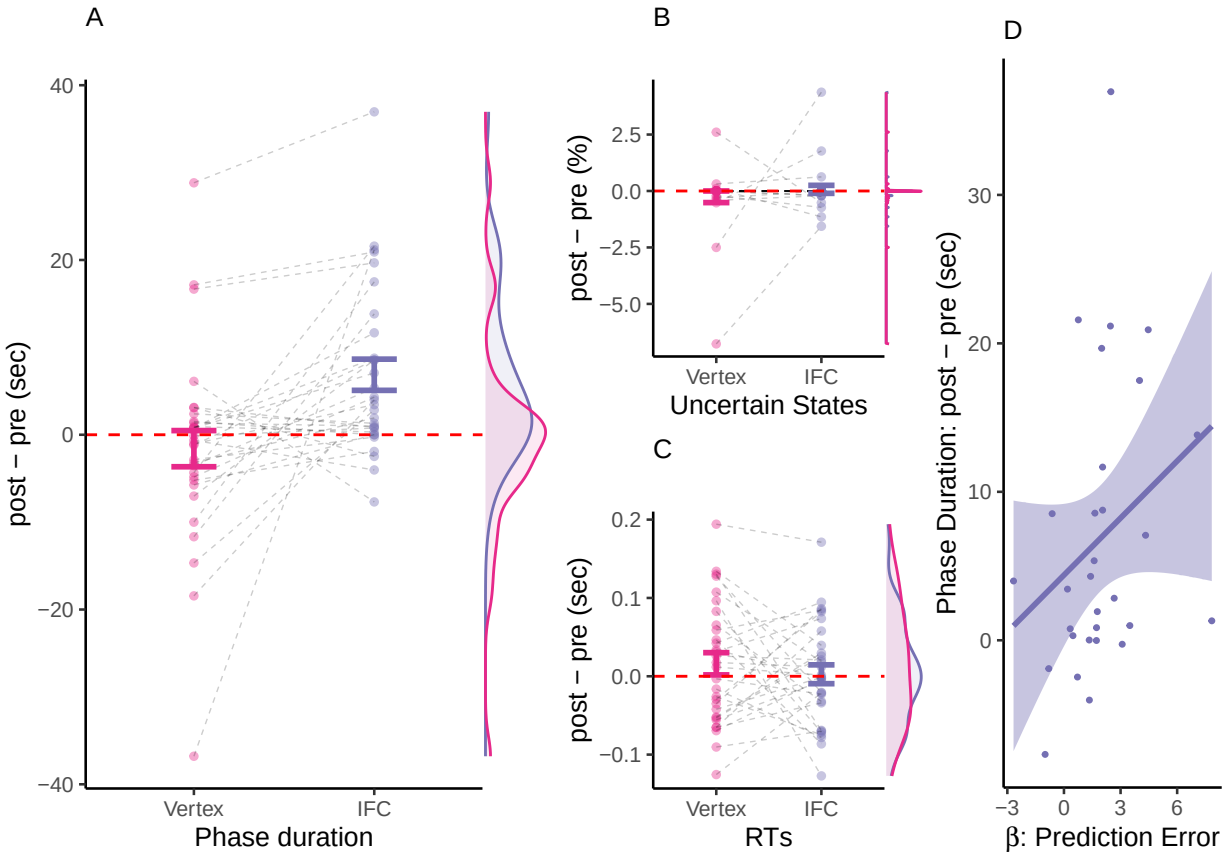

Figure 4. TMS effects on perception. A. Phase duration. Here, we depict the impact of virtual lesions in vertex and IFC on conflict-driven changes in conscious experience in terms of differences in phase duration (post- vs. pre-stimulation). Marginal densities are shown on the right. Virtual IFC-lesions prolonged phase durations (post-pre: 6.86 ± 1.79 sec) relative to the vertex condition (−1.59 ± 2.07 sec; paired t-test: T(29) = -3.44, p = 1.77×10^{-3}, $BF_{10} = 20.05$). **B. Unclear perceptual states.** TMS to IFC did not alter the frequency of uncertain perceptual states (post-pre: 0.07 ± 0.18%) in comparison to the TMS to vertex (−0.26 ± 0.26%; paired t-test: T(29) = -1.04, p = 0.31, $BF_{10} = 0.32$). **C. Response times.** Virtual IFC-lesions did not affect RTs (post-pre: 2.55×10^{-3} ± 0.01 sec) in comparison to control stimulation at vertex (0.02 ± 0.01 sec; paired t-test: T(29) = 0.77, p = 0.45, $BF_{10} = 0.26$). **D. Representation of perceptual conflict and virtual lesions in IFC.** Participants who represented perceptual conflict more strongly in IFC (correlation coefficient β of perceptual prediction errors to BOLD signals in individual IFC stimulation

sites; GLM-PC) showed an enhanced reduction of conflict-induced changes in conscious experience when neural activity in IFC was disrupted by TMS ($\rho = 0.42$, $p = 0.02$).

9 Tables

GLM-PC (p < 0.05 FWE)

Region	E1	x(E1)	y(E1)	z(E1)	T(E1)	E2	x(E2)	y(E2)	z(E2)	T(E2)
Overlaps										
V1-V5: L		-21	-97	8	13.76		18	-97	11	15.16
V1-V5: R		21	-94	11	14.26		-18	-100	8	13.60
SPL: L		-24	-58	59	5.67		-24	-61	59	6.66
SPL: R		24	-52	59	7.22		27	-52	53	7.64
IPL: L(o)							-30	-49	53	7.19
Transitions										
Cerebelum: L		-27	-61	-19	8.43					
Cerebelum: R		21	-49	-22	11.57		21	-52	-22	8.09
Precentral: L		-42	-22	62	10.06		-30	-19	65	6.95
Postcentral: L		-39	-28	50	8.64		-42	-28	53	7.94
MCC: L		-6	11	35	6.16		-3	-1	56	6.12
MCC: R		12	17	32	6.57					
Putamen: L		-21	11	-1	7.52					
Putamen: R		21	14	2	6.51					
Insula: L(t)		-39	-4	11	6.60					
IPL: L		-51	-28	26	6.28					
MFG: L		-36	41	26	6.64					
Prediction Errors										
Insula: L		-30	23	-1	8.21					
Insula: R		33	23	-1	7.57		33	20	-1	7.38
IFG: R		45	17	23	5.61		48	20	2	6.57
hMT+: R		45	-64	8	5.89		48	-58	5	6.46
IPL: R		39	-37	50	6.03					
PMF: R		3	23	50	5.72		6	17	56	6.55

Table 1. The neural correlates of perceptual conflict. Here, we summarize the fMRI results for GLM-PC (experiments E1 and E2, all $p_{FWE} < 0.05$). Visual stimulation ("Overlaps") correlated with BOLD signals throughout visual cortex (including V5/hMT+), bilateral superior parietal lobulus (SPL) and inferior parietal lobulus (IPS). At the time of perceptual events, we found *change-related* activations in bilateral cerebellum, left pre- and postcentral gyrus, bilateral midcingulate cortex and putamen, left insula, left IPL as well as left medial frontal gyrus (MFG). Perceptual prediction errors (i.e., the quantitative

representation of perceptual conflict) correlated with BOLD signals in bilateral insula, right inferior frontal gyrus (IFG), right V5/hMT+, right IPL and right posterior-medial frontal gyrus (PMF).

GLM-Congruency (p < 0.05 FWE; *SCV within the main effect of Congruency)

Region	Congruency	x(M)	y(M)	z(M)	F(M)	Congruency x Signal-to-Ambiguity	x(I)	y(I)	z(I)	F(I)
IFG: R		45	23	29	31.30		45	17	26	5.69*
Insula: R		33	23	5	23.14		33	23	2	5.30*
hMT+: R		45	-61	5	23.57		48	-64	8	5.63*
Precentral: L		-42	-4	38	35.05		-42	-4	35	5.54*
PMF: R		6	17	50	31.66		6	14	47	5.87*
Fusiform: R		33	-67	-10	24.20		33	-67	-10	4.67*
V1: L							-15	-73	5	7.19
V1: R							15	-70	8	8.23

Table 2. The neural correlates of graded ambiguity. To test the relation of V5/hMT+ and IFC to perceptual conflict during graded ambiguity, we modeled congruent and incongruent perceptual states by box-car regressors, separately for all six levels of signal-to-ambiguity. Group results were assessed using second-level ANOVA for the factors *Congruency* and *Signal-to-Ambiguity*. We found a main effect of *Congruency* (i.e., enhanced BOLD signals during incongruent as opposed to congruent perceptual states; $p_{FWE} < 0.05$) in right-hemispherical IFC (insula and inferior frontal gyrus), V5/hMT+, left precentral gyrus, right posterior-medial frontal gyrus (PMF) and right fusiform gyurs. We did not find any whole-brain correctable main effect of *Signal-to-Ambiguity*. Within the main effect of *Congruency* (thresholded at $p_{FWE} < 0.05$), the interaction between *Congruency* and *Signal-to-Ambiguity* was significant in right-hemispherical IFC (insula and inferior frontal gyrus), V5/hMT+, left precentral gyrus, right PMF and right fusiform gyrus. Two additional cluster for this interaction in bilateral V1 ($p_{FWE} < 0.05$) did not show a main effect of *Congruency*.

10 Supplementary materials

10.1 Stimulus characteristics

In this work, we elicited bistable perception by presenting a discontinuous structure-from-motion stimulus (Supplementary Video S1). Experiments E1 and E3 used fully ambiguous versions of the stimulus and were conducted in the same sample of participants. In E2, the stimulus was either fully ambiguous or parametrically disambiguated (*graded ambiguity*). In each study sample, we also collected data for one run of fully disambiguated structure-from-motion stimuli alternating at a probability of 15% per overlapping configuration. These control runs allowed us to assess (i) whether participants followed the experimental instructions during ambiguity and (ii) whether there was a difference in the frequency of unclear perceptual states between fully ambiguous and fully disambiguated stimuli. Here, we assess the characteristics of the structure-from-motion stimulus across experiments E1, E2 and E3 (see Main Text for data on *phase duration* and *RTs*).

Individual participants showed small but significant *biases* toward one of the two perceptual alternatives: The more prevalent alternative accounted for 64.87 ± 1.07% of perceptual states (*absolute bias*, T(54) = 13.88, p = 1.9×10^{-19}, $BF_{10} = 2.66 \times 10^{16}$; one-sample t-test). Across participants, however, none of the two perceptual alternatives was preferred over the other (*directed bias*): 48.47 ± 1.01% of perceptual states were assigned to rightward rotation of the sphere (T(54) = -1.5, p = 0.14, $BF_{10} = 0.42$).

Unclear perceptual states were rare (0.6 ± 0.18%) and more frequent in comparison to a disambiguated control stimulus (0.04 ± 0.03%; T(54) = 3.13, p = 2.81×10^{-3}, $BF_{10} = 11$; paired t-test). Accuracy of perceptual reports for this disambiguated stimulus was high (96.75 ± 1.42%), indicating that participants followed the experimental instructions.

10.2 The predictive-coding model of bistable perception

In this work, we investigated how neural activity in IFC related to the perceptual conflict inherent in ambiguous sensory information. Next to a *standard* assessment of perceptual conflict (see GLM-Congruency, E2), we applied an established *computational model* of bistable perception[23,43,74]. By inverting this model, we estimated perceptual prediction errors as a quantitative representation of perceptual conflict.

In this supplement, we provide a mathematical description of the computational model of bistable perception. In addition, we describe how the model was inverted based on behavioral data. In simulation analyses, we illustrate the relation between model parameters (π_{IPS}: the initial belief in the stability of the visual environment; π_{ERROR}: the impact of perceptual conflict on the belief in the stability of the visual environment; π_{DIS}: the participants' sensitivity to disambiguating stimulus information) and the temporal characteristics of conscious experience y. With this, we derive quantitative predictions for the behavioral and imaging analyses outlined in the Results section.

10.2.1 Model description

Throughout the experiments E1 to E3, we presented a rotating discontinuous structure-from-motion stimulus. Participants reported whether they perceived the front surface of the object as rotating to the left or right. During full ambiguity, the direction of rotation spontaneously changed at a specific frequency (phase duration) in each participant. During graded ambiguity[43], we experimentally manipulated the stimulus by introducing *disambiguating stimulus information* in form of 3D cues. Depending on the signal-to-ambiguity ratio, this disambiguating stimulus information biased conscious experience toward stimulus-congruent perceptual states.

Here, we explain how sensory data and implicit beliefs about the stability of the sensory environment give rise to perceptual states y during full and graded ambiguity. We adopt a

Bayesian approach assuming that perceptual states are determined by *posterior probability distributions*. Posterior probability distributions result from the combination of currently available sensory data (the *likelihood distribution*) with information acquired from previous visual experience (the *prior distribution*).

During full ambiguity, our model assumes a bi-modal likelihood distribution representing balanced evidence for both perceptual interpretations. Graded ambiguity shifts the balance of the likelihood in the direction of one perceptual interpretation at the expense of the other. In this context, sensory information is described by the direction of disambiguation (μ_{DIS}) and the amount of disambiguation (i.e., the *signal-to-ambiguity* ratio; defined for the condition D1-D6 of experiment E2). As a free parameter, π_{DIS} reflects the individual impact of disambiguating stimulus information on conscious experience. This is equivalent to the participants' sensitivity to disambiguating stimulus information during graded ambiguity.

The prior, in turn, is modeled as a uni-modal distribution centered on the previously dominant perceptual interpretation. It acts as an implicit belief in the stability of the environment. The prior is defined by the current perceptual state ($\mu_{stability}$) and its impact on future conscious experience ($\pi_{stability}$). Two free parameters define the the temporal evolution of $\pi_{stability}$: π_{IPS} reflects the maximum value of $\pi_{stability}$, which we allocate to the beginning of a perceptual phase. In addition, we assume that $\pi_{stability}$ decays linearly during a perceptual phase. This linear decay (with a lower bound at 0) occurs relative to the impact (or *precision*) of perceptual prediction errors (π_{ERROR}, see below).

The model combines bimodal likelihood and unimodal stability prior. This computes the available evidence for both interpretations of the sensory data. Crucially, once a percept is established, the residual evidence for the suppressed perceptual state constitutes a perceptual prediction error. Relative to the precision of the prediction error (π_{ERROR}), this quantitative representation of perceptual conflict leads to a linear reduction in the precision of the stability prior. Over time, this results in escalating prediction errors and a dynamic shift of the

posterior distribution toward the currently suppressed perceptual interpretation. This entails an increasing probability of a change in conscious experience. Once the change has occurred, the stability prior shifts to the now-dominant stimulus interpretation and its precision is re-set to an initial value (π_{IPS}). As predicted by predictive-coding theories of perceptual inference[20,33], prediction errors are thus minimized after the observer adopts a new perceptual interpretation.

In addition, our model assumes a modulation of prediction error accumulation by disambiguating stimulus information: When the current perceptual state is congruent with the disambiguating sensory evidence, our model predicts that prediction errors are reduced relative to full sensory ambiguity. Conversely, when perception is incongruent with the disambiguating sensory evidence, our model assumes enhanced perceptual prediction errors. Importantly, the strength of this enhancement/reduction in prediction errors scales with the amount of sensory evidence during graded ambiguity (i.e., the *signal-to-ambiguity* ratio) and the participants' sensitivity to disambiguating stimulus evidence (π_{DIS}).

Hence, three free parameters control the perceptual dynamics produced by our model: The intial precision of the stability prior π_{IPS}, the precision of perceptual prediction errors π_{ERROR}, which governs the rate of linear decay in the precision of the stability prior over time, and, in the case of graded ambiguity, the participants' sensitivity to disambiguating stimulus evidence π_{DIS}. We infer these parameters by inverting our model based on the sequence of percepts y indicated by the participants and, in the case of graded ambiguity, the available sensory information (μ_{DIS}: direction of disambiguation; SAR: signal-to-ambiguity ratio)

Since changes in conscious experience for non-depth-symmetrical structure-from-motion stimuli occur exclusively at overlapping stimulus configurations[24,30], we represent percepts and all further model quantities in discrete time points t defined by stimulus overlaps. For computational expediency, our model assumes Gaussian probability distributions defined by mean and precision (inverse of variance).

At each timepoint t, we compute the probability of the two percepts based on the posterior distribution $P(\theta)$:

$$\theta = \begin{cases} > 0.5: & \rightarrow \quad (rotation) \\ < 0.5: & \leftarrow \quad (rotation) \end{cases} \tag{1}$$

The currently perceived direction at timepoint t is defined by:

$$y(t) = \begin{cases} 1: & \rightarrow \quad (rotation) \\ 0: & \leftarrow \quad (rotation) \end{cases} \tag{2}$$

We manipulate the level of sensory information by changing the fraction of dots associated with a stereo-disparity signal. This is captured by a Gaussian distribution *Disambiguation* ($\mathcal{N}(\mu_{DIS}, \pi_{DIS}^{-1})$). The direction of disambiguation at timepoint t is represented by μ_{Dis}:

$$\mu_{Dis}(t) = \begin{cases} 1: & \rightarrow \quad (disambiguation) \\ 0.5: & \leftrightarrow \quad (ambiguous) \\ 0: & \leftarrow \quad (disambiguation) \end{cases} \tag{3}$$

π_{DIS} represents the participants' sensitivity to disambiguating stimulus information. The amount of disambiguating stimulus information was varied systematically in 120 sec blocks of visual stimulation. The signal-to-ambiguity ratio (SAR) was defined by the fraction of stimulus dots that carried a 3D cue (level **D1**: 0.15, **D2**: 0.30, **D3**: 0.45, **D4**: 0.60, **D5**: 0.75

and **D6**; 1.00). If set to zero, π_{DIS} is removed from the model.

$$\pi_{Graded} = \pi_{DIS} * SAR \tag{4}$$

Furthermore, our model assumes that an implicit prior belief in the stability of the visual environment controls the frequency of changes in conscious experience during bistability. The mean of the Gaussian distribution "stability" ($\mathcal{N}(\mu_{stability}, \pi^{-1}_{stability})$) is determined by the perceptual state indicated by the participants at the overlap preceding timepoint t:

$$\mu_{stability}(t) = y(t-1) \tag{5}$$

$\pi_{stability}$ describes the impact of the "stability" prior on perceptual state. If a change in conscious experience occurred at the preceding overlap ($t = t_0$), $\pi_{stability}(t)$ is set to the initial stability precision π_{IPS}:

$$\pi_{stability}(t = t_0) = \pi_{IPS} \tag{6}$$

Inversion of our model during graded ambiguity allows for the estimation of π_{IPS}. If fixed to zero, the parameter is removed from the model.

If no perceptual event occurred at the preceding overlap ($t \neq t_0$), we calculate $\pi_{stability}(t)$ by updating the previous precision of the stability prior $\pi_{stability}(t-1)$ with a precision-weighted

prediction error (PE). The precision of the prediction error (π_{ERROR}) reflects how quickly $\pi_{stability}$ decays over time and is estimated as a free parameter:

$$\pi_{stability}(t \neq t_0) = \pi_{stability}(t-1) - \pi_{ERROR} * |PE(t-1)| \tag{7}$$

By combining the stability prior ($\mathcal{N}(\mu_{stabiliy}, \pi^{-1}_{stability})$) with the signal-to-ambiguity-adjusted likelihood ($\mathcal{N}(\mu_{DIS}, \pi^{-1}_{Graded})$), we adjust the density ratio r of the posterior $P(\theta)$ for the two peak locations $\theta_0 = 0$ and $\theta_1 = 1$:

$$m(t) = \frac{\pi_{stability} * \mu_{stability}(t) + \pi_{graded} * \mu_{DIS}(t)}{\pi_{stability} + \pi_{graded}} \tag{8}$$

$$r(t) = exp(\frac{(\theta_1 - m(t))^2 - (\theta_0 - m(t))^2}{2 * (\pi_{stability} + \pi_{graded})^{-2}}) \tag{9}$$

The posterior probability of right-ward rotation predicts the perceptual response $y(t)$:

$$y_{predicted}(t) = \frac{1}{r(t) + 1} \tag{10}$$

We infer on the free parameters (π_{DIS}, π_{ERROR}, π_{IPS}) by optimizing the model with regard to the difference between the prediction and the actual perceptual response ($y_{predicted}$ and y). Once a new percept $y(t)$ has been established, we compute the residual evidence

for the alternative perceptual interpretation. This model quantity reflects a quantitative representation of dynamic changes in perceptual conflict. Given the inspiration of our model by predictive coding, we refer to this quantity as the *perceptual prediction error* $PE(t)$:

$$PE(t) = y(t) - y_{predicted}(t) \tag{11}$$

10.2.2 Model inversion

For model inversion, we used a free energy minimization approach[75], which maximised a lower bound on the log-model evidence for the individual participants' data. We modeled π_{IPS}, π_{ERROR} and π_{DIS} either as free parameters defined by log-normal distributions or fixed these entities to zero, thereby effectively removing them from the model. We optimised parameters using quasi-Newton Broyden-Fletcher-Goldfarb-Shanno minimisation as implemented in the HGF3.0 toolbox (TAPAS toolbox, http://www.translationalneuromodeling.org/hgf-toolbox-v3-0/).

For ambiguous visual stimulation, parameters were inverted using the following priors: π_{IPS} = prior mean of log(2) and prior variance of 1; π_{ERROR} = prior mean of log(1) and prior variance of 0.1. For graded ambiguity, prior means for π_{IPS} and π_{ERROR} were defined by the posterior estimates obtained from the preceding ambiguous runs. Prior variance was reduced to 0.01 for π_{IPS} and to 0.001 for π_{ERROR}. π_{DIS} was estimated with a prior mean of log(2) and a prior variance of 1.

We used the inverted models for model-based fMRI in experiment E1 (posterior parameter estimates: $\pi_{IPS} = 2.83 \pm 0.22$; $\pi_{ERROR} = 0.7 \pm 0.08$) and E2 ($\pi_{IPS} = 2.25 \pm 0.13$; $\pi_{ERROR} = 0.57 \pm 0.09$; $\pi_{DIS} = 1.05 \pm 0.15$). Relative to model variants in which free parameters were systematically removed, models incorporating the full set of parameters (Ambiguity:

π_{IPS} and π_{ERROR}, Graded ambiguity: π_{IPS}, π_{ERROR} and π_{DIS}) were superior in explaining the participants' behaviour (protected exceedance probability E1: 100%; E2: 99.98%). Furthermore, posterior model parameters were uncorrelated, indicating successful model inversion in E1 (π_{IPS} to π_{ERROR}: ρ = -0.18, $p = 0.32$) and E2 (π_{IPS} to π_{ERROR}: ρ = -0.35, $p = 0.13$; π_{IPS} to π_{DIS}: $\rho = 0.17$, $p = 0.47$; π_{ERROR} to π_{DIS}: $\rho = 0.3$, $p = 0.2$).

Based on previous work[23], our model-based fMRI approach focused on perceptual prediction errors, since this model quantity provides a dynamic and quantitative representation of perceptual conflict.

10.2.3 Simulation

To visualize the predictions of our model, we simulated experiment E2 (one run of ambiguous stimulation; three runs of graded ambiguity across six levels of sensory evidence D1 to D6) for a total of 100 hypothetical participants. Parameters for simulation were drawn randomly between the 30% and 70% quantile of posterior parameters estimated in the behavioral pretest ($\pi_{IPS} = 2.23 \pm 0.14$, $\pi_{ERROR} = 0.36 \pm 0.07$; $\pi_{DIS} = 1.73 \pm 0.30$).

As expected, the distribution of simulated phase durations (Supplementary Figure S8A) obtained during ambiguous stimulation showed a sharp rise and long tail. It was best fit by a gamma distribution (Bayesian Information Criterion = 3.83×10^4; shape = 1.66, rate = 0.14) as compared to a lognormal (BIC = 3.85×10^4) and a normal distribution (BIC = 4.11×10^4).

When simulating graded ambiguity, we observed that disambiguating stimulus information biased the model predictions toward congruent perceptual states (Supplementary Figure S8B). This congruency effect was stronger at higher levels of signal-to-ambiguity (F(495) = 195.1, p = 1.49×10^{-114}, $BF_{10} = 4.23 \times 10^{120}$). Simulated prediction errors signaled elevated perceptual conflict during incongruent as opposed to congruent perceptual states (main effect of *Congruency*: F(1.09×10^3) = 4.15×10^3, p = 0, $BF_{10} = 6.7 \times 10^{275}$, Figure S8C).

Differences in prediction errors between congruent and incongruent perceptual states scaled with the signal-to-ambiguity ratio (interaction between *Congruency* and *Signal-to-Ambiguity*: $F(1.09 \times 10^3) = 148.71$, $p = 2.1 \times 10^{-120}$, $BF_{10} = 1.97 \times 10^{116}$). We also observed a main effect of *Signal-to-Ambiguity* ($F(1.09 \times 10^3) = 81.43$, $p = 1.07 \times 10^{-72}$, $BF_{10} = 1.14 \times 10^{42}$).

Thus, when simulating from this computational model, we observed that the model's predictions closely followed the behavioral characteristics of both full and graded ambiguity.

10.3 Decoding the contents of conscious experience

We used multi-variate pattern analysis to isolate brain regions that contained information about the dynamic *contents of conscious experience*. This was achieved in a standard cross-validated leave-one-run-out searchlight decoding analysis[76]. This approach classified between two regressors that represented the alternative stimulus interpretations, i.e., leftward and rightward rotation. Thereby we predicted, based on brain activity, which of the two perceptual states was dominant or suppressed at a given point in time. In both experiments E1 and E2, searchlight analysis was carried out with a radius of 8 voxels (unsmoothed data), using a support vector machine[77] as a binary classifier.

In both experiments, information about the current content of conscious experience was primarily represented in visual and parietal brain region (Supplementary Figure S6A). To test whether the representation of perceptual conflict in IFC and V5/hMT+ overlapped with brain regions that contained information about the current content of conscious experience, we computed average classification accuracy in voxels within V5/hMT+ and IFC (see section 7.3.4 for ROI-definition).

Classification accuracy was significantly above chance in V5/hMT+ for data from both E1 ($T(31) = 2.35$, $p = 0.03$, $BF_{10} = 2.03$) and E2 ($T(19) = 3.02$, $p = 6.97 \times 10^{-3}$, $BF_{10} = 6.93$, Supplementary Figure S6B). In IFC, we found no conclusive evidence for above-chance classification in E1 ($T(31) = 1.95$, $p = 0.06$, $BF_{10} = 1$) or E2 ($T(19) = 1.92$, $p = 0.07$, BF_{10}

= 1.08). Hence, reliable decoding of the contents of conscious experience was possible for V5/hMT+, but not IFC.

10.4 Perceptual uncertainty and temporal balances during graded ambiguity

Our imaging analysis of E2 strongly suggested that IFC detected dynamic changes in perceptual conflict during graded ambiguity. In addition to model-based fMRI, this interpretation was supported by IFC reflecting both a main effect of *Congruency* and an interaction between *Congruency* and *Signal-to-Ambiguity*. Here, we provide additional control analyses to rule out that differences in perceptual uncertainty and temporal imbalance of perceptual states at different levels of *Signal-to-Ambiguity* may have confounded these fMRI results.

Firstly, since previous research has associated IFC with unclear percepts during bistability[26], we asked whether differences in perceptual uncertainty between congruent and incongruent perceptual states could provide an alternative interpretation of our findings. In experiment E2, unclear perceptual states were extremely rare ($0.29 \pm 0.13\%$) and unaffected by levels of *Signal-to-Ambiguity* ($F(95) = 1.4$, $p = 0.23$), indicating that participants were able to discriminate between the alternative stimulus interpretations at all times. In an additional control experiment (Run 3 of E2, Supplementary Figure S1B), we obtained ratings of perceptual uncertainty associated with congruent and incongruent perceptual states (Supplementary Figure S8). Perceptual uncertainty was low for both congruency (average rating: 1.2 ± 0.05, range: 1 to 4) and incongruency (1.4 ± 0.06) to disambiguating stimulus information. Incongruent perceptual states were associated with an increase in perceptual uncertainty (Chi-square = 19.43, $p = 3.5 \times 10^{-3}$, $BF_{10} = 27.3$). Importantly, however, such differences in perceptual uncertainty were unaffected by levels of *Signal-to-Ambiguity* (Chi-square = 7.41, $p = 0.19$, $BF_{10} = 5.53 \times 10^{-5}$).

Secondly, we asked whether the temporal imbalance between congruent and incongruent

perceptual states might have confounded our imaging results. In a fMRI control experiment (Run 8 of E2, Supplementary Figure S1B), participants reported the direction of motion (left vs. right) of unambiguous 2D dot fields. Across six levels of *Temporal Imbalance*, we matched the *Relative Duration* of perceptual outcomes to the effects of signal-to-ambiguity on perceptual congruency. Even at a lenient threshold of $p < 0.001$ (uncorrected voxel-wise whole-brain analysis), we did not observe a main effect of *Relative Duration* or an interaction between *Relative Duration* and *Temporal Imbalance* in any of the regions implicated in the representation of perceptual conflict.

In sum, neither differences in perceptual uncertainty nor temporal imbalances between congruent and incongruent perceptual states provided alternative explanations for the modulation of neural activity in V5/hMT+ and IFC by perceptual conflict.

10.5 Effects of TMS on the stability, the uncertainty and the report of conscious experience during bistable perception

In our analysis of E3, we have focused on differences in phase duration, unclear perceptual states and RTs associated with TMS to either IFC or vertex. We observed that TMS-induced virtual lesions in IFC were associated with a pronounced prolongation of phase durations. Importantly, we found no evidence for an influence of IFC on either the uncertainty or the report of perceptual states.

Here, we confirmed these results in linear mixed effects modeling. To this end, we analyzed the counter-balanced TMS experiment with respect to two factors: *Session* (IFC vs. vertex) and *Stimulation* (post vs. pre). We used linear mixed effects modeling (lmer R-package) with fixed effects for *Session* and *Stimulation*. Random effects were defined for individual participants.

The relative prolongation of phase durations after TMS to IFC was reflected by a significant interaction between the factors *Stimulation* and *Session* ($F(87) = 6.35$, $p = 0.01$, $BF_{10} =$

3.75). We did not observe a main effect of *Stimulation* (F(87) = 2.47, p = 0.12, $BF_{10} = 0.49$) or *Session* (F(87) = 0.11, p = 0.29, $BF_{10} = 0.2$; Supplementary Figure S1D).

With respect to unclear perceptual states (Supplementary Figure S10), we found no main effect of *Session* (F(58) = 0.34, p = 0.56, $BF_{10} = 0.49$) or *Stimulation* (F(58) = 0.35, p = 0.56, $BF_{10} = 0.24$) and no between-factor interaction (F(58) = 1.12, p = 0.3, $BF_{10} = 0.31$). Likewise, when assessing a potential modulation of RTs by TMS (Supplementary Figure S3D), we found no main effect *Session* (F(58) = 0.07, p = 0.8, $BF_{10} = 0.21$) nor *Stimulation* (F(58) = 0.07, p = 0.79, $BF_{10} = 0.24$) nor a between-factor interaction (F(58) = 0.52, p = 0.47, $BF_{10} = 0.31$).

Linear mixed effects modeling thus corroborated that TMS-induced virtual lesions in IFC had a selective effect on the occurrence of changes in conscious experience during bistable perception.

10.6 Effects of stimulus exposure on the dynamics of conscious experience

In binocular rivalry, changes in conscious experience evoked by binocular conflict have been shown to occur more frequently when participants were exposed to the sensory ambiguity repeatedly over several days[78]. Likewise, in E1 and E3, we observed a shortening of phase durations elicited by structure-from-motion with increasing stimulus exposure (F(321.65) = 5.9, p = 9.71×10^{-9}, $BF_{10} = 1.18 \times 10^{6}$; see Supplementary Figure S2C).

To make sure that the effects attributed to TMS-induced virtual lesions were not confounded by this effect of exposure, we re-analyzed the behavioral data from the counter-balanced TMS-experiment with respect to three factors: *Exposure* (increasing from Run 1 to Run 8), *Session* (IFC vs. vertex) and *Stimulation* (post vs. pre).

Linear mixed effects modeling confirmed the main effect of stimulus exposure on phase duration (F(202.03) = 14.43, p = 1.93×10^{-4}) in the course of the TMS-experiment. As a

reflection of the effect of TMS on the stability of conscious experience, we found a highly significant interaction between the factors *Session* (IFC vs. vertex) and *Stimulation* (post vs. pre; F(202.03) = 11.53, p = 8.25×10^{-4}), a main effect of *Stimulation* (F(202.03) = 4.85, p = 0.03), but no main effect of *Session* (F(202.03) = 0.12, p = 0.73). However, the effects of *Exposure* were independent of the effects of *Stimulation* and *Session* (BF_{10} = 26.33). Linear mixed effects modeling did not reveal a two-way interaction between the factors *Exposure* and *Session* (F(202.03) = 0.03, p = 0.87) or *Stimulation* (F(28.01) = 3.73×10^{-3}, p = 0.95) and no three-way interaction (F(202.03) = 0.28, p = 0.59).

We thus did not observe any evidence for a confounding of TMS-related effects by effects introduced by stimulus exposure.

10.7 Regression toward the mean

As a consequence of the independence between the long-term speeding induced by stimulus exposure and the IFC-TMS-induced stabilization of conscious experience, pre-stimulation phase duration differed between vertex- and IFC- in runs E3(5) (IFC: 19.82 ± 3.69 sec; vertex: 25.22 ± 4.65 sec; one-sided two-sample t-test: T(26.63) = -0.91, p = 0.19) and E3(6) (IFC: 19.38 ± 4.83 sec; vertex: 24.09 ± 4.06 sec; T(26.52) = -0.75, p = 0.23). One may thus assume that, by virtue of *regression toward the mean* (RTM), such differences at baseline might have confounded our analyses of TMS-related effects.

However, due to the high correlation between pre- and post-TMS-measurements, variance attributable to RTM (i.e., $100 * (1 - \rho_{Spearman})\%$) was low for TMS to both vertex (13.26%) and IFC (11.43%). As an additional control analysis, we applied Mee and Chua's test[79] to differentiate between the RTM effect and additional TMS effects τ. For TMS to IFC, we found significant TMS effects over and above RTM estimated τ = 7.98 sec; T = 4.83, p = 4.38×10^{-5}). As expected, control stimulation to the vertex was not associated with any significant additional effects on phase duration (estimated τ = -1.53 sec; T = -0.73, p = 0.47).

In sum, these analyses provided strong evidence against a potential confound of the observed TMS effects by RTM.

10.8 Supplementary Figures

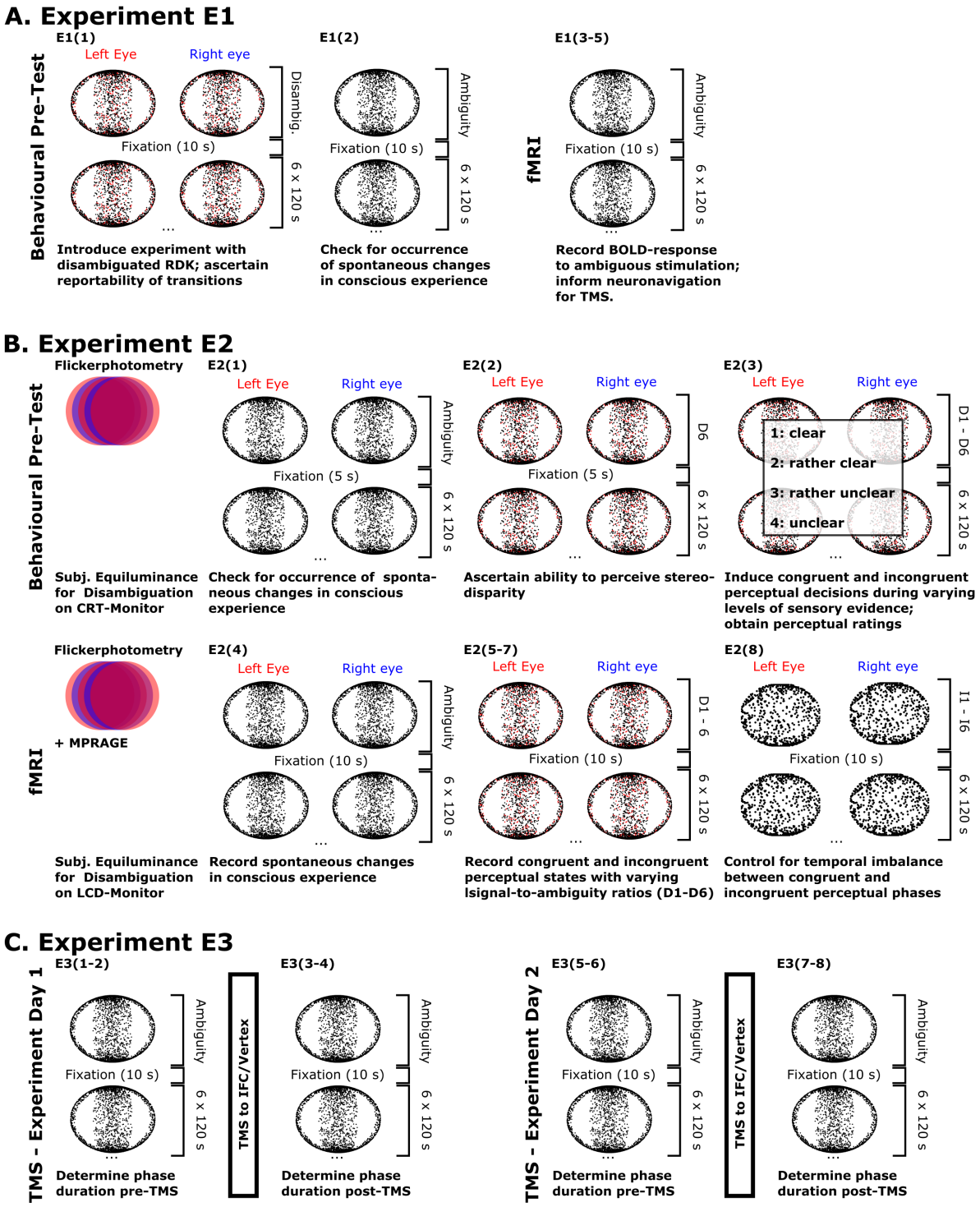

Supplementary Figure S1. Experimental Paradigm. A. Experiment E1. In E1, we investigated how IFC responded to the perceptual conflict inherent in ambiguous

visual stimulation. The experimental protocol started with a behavioral pre-test, which familiarized the participants with the experiment. **Run 1** tested adequate performance in reporting changes in direction of rotation of a fully disambiguated RDK (probability: 15% per overlapping configuration). **Run 2** checked whether participants perceived spontaneous changes in conscious experience during ambiguous visual stimulation. In a separate experimental session, we collected fMRI-data during three runs of ambiguous structure-from-motion (**Runs 3-5**). This allowed us to assess how IFC responded to the perceptual conflict during bistable perception. In addition, the fMRI data were used to localize change-related BOLD activity in IFC for neuronavigated inhibitory TMS (see E3). **B. Experiment E2.** In E2, we tested how neural activity in IFC responded to varying levels of sensory ambiguity. In a behavioral pretest, we tested whether participants perceived a sufficient number of changes in conscious experience during full ambiguity (**Run 1**) and assessed their ability to perceive 3D cues during full disambiguation (**Run 2**). **Run 3** introduced graded ambiguity. Here, a fraction of the dots composing the RDK (highlighted in red) were shifted between the two monocular channels. The conditions D1 to D6 were defined by the percentage of disambiguated dots (signal-to-ambiguity ratio, 15%, 30%, 45%, 60%, 75% and 100%) and occurred in random order. We determined the frequency of exogenous stimulus changes during graded ambiguity based on the frequency of changes in conscious experience during full ambiguity. In Run 3, we tested the effects of signal-to-ambiguity on the proportion of perceptual states congruent to the disambiguating stimulus information. Moreover, we obtained ratings of perceptual uncertainty for both congruent and incongruent perceptual states across six levels of signal-to-ambiguity. To test for effects of signal-to-ambiguity on neural activity in IFC, we measured BOLD activity during one run of full ambiguity (**Run 4**) and three runs of graded ambiguity (**Runs 5-7**). In **Run 8**, we conducted a final control experiment assessing the effects of temporal imbalance introduced between congruent and incongruent perceptual states across conditions D1-D6. Here, we presented leftward and rightward planar dot motion in six conditions of

increasing temporal imbalance (I1-I6). All experiments in E2 used filter-glasses to present 3D stimuli. We adjusted the subjective luminance of the red (left eye) and blue (right eye) channel using heterochromatic flicker photometry. **C. Experiment E3.** E1 and E2 established that neural activity in right-hemispheric IFC signals the accumulating conflict between conscious experience and the underlying sensory information. In E3, we probed a causal contribution of IFC activity to conscious experience. We re-invited the participants of E1 to two additional TMS-session scheduled on consecutive days (Day 1: **Runs 1-4**; Day 2: **Runs 5-8**). Using online neuronavigation based on the fMRI experiment in E1, we created virtual lesions in IFC and a control region at the cranial vertex (order counter-balanced across participants). We assessed the effects of virtual lesions on the dynamics and content of conscious experience by comparing pre- with post-stimulation runs.

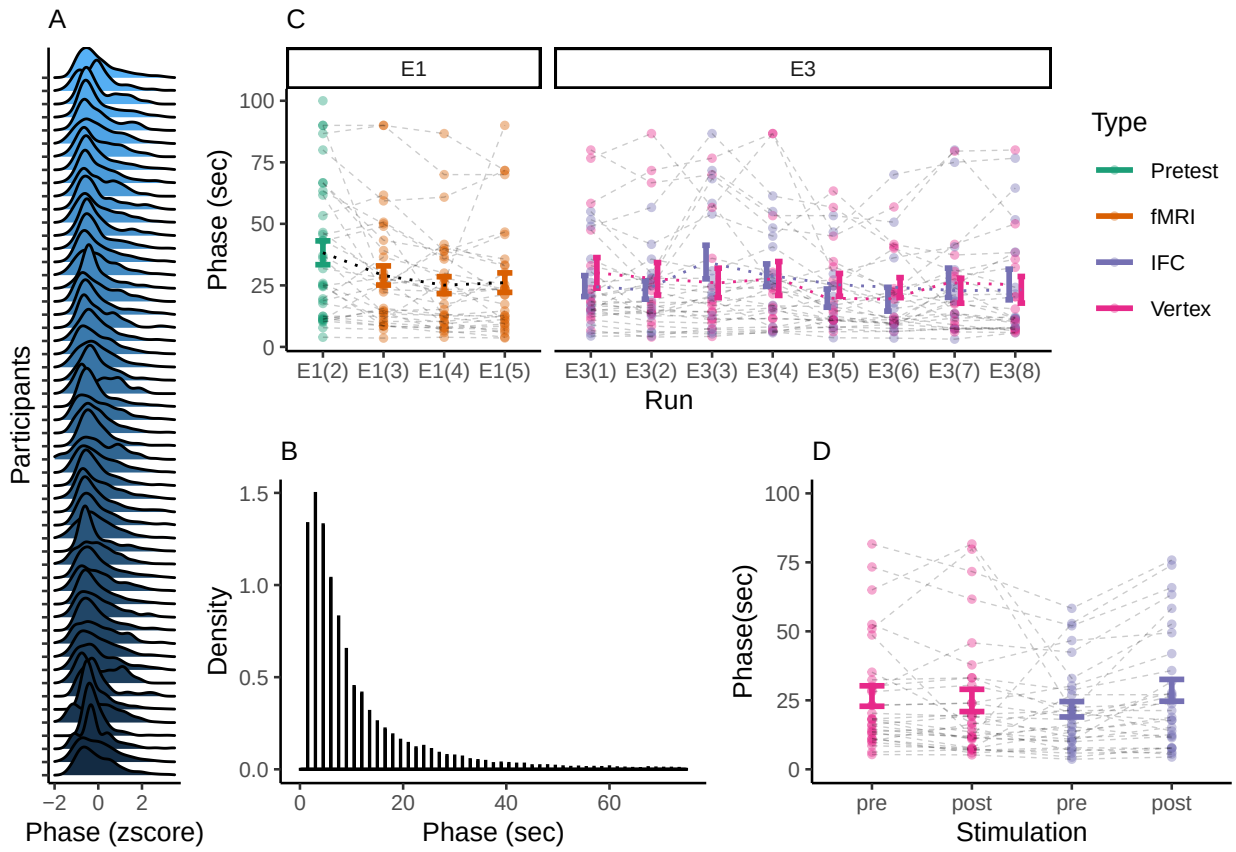

Supplementary Figure S2. Phase Duration. A. Individual distributions of phase duration. In individual participants (E1-E3), the distribution of phase durations (z-scored for visualization) followed the sharp rise and long tail that is typically observed in perceptual bistability. **B. Aggregated phase durations.** When aggregated across participants, the distribution of phase durations (multiples of the 1.5 sec inter-overlap interval) was again characterized by a sharp rise and long tail. This pattern was best fit by a log-normal distribution (Bayesian Information Criterion = 1.79×10^5; log(mean) = 1.91, log(sd) = 0.95) as compared to a gamma (BIC = 1.85×10^5) and a normal distribution (BIC = 2.18×10^5). **C. Effects of stimulus exposure on phase duration.** Across the experimental runs of E1 and E3, we observed a significant decrease in phase duration with increasing exposure to the bistable stimulus (F(321.65) = 5.9, p = 9.71×10^{-9}, $BF_{10} = 1.18 \times 10^6$; see dotted lines). When assessing the evolution of phase duration across the counter-balanced TMS-experiment (E3; blue dotted line: IFC-stimulation first; red dotted line: vertex-stimulation first), linear

mixed effects modeling again showed a main effect of *Exposure* ($F(202.03) = 14.43$, $p = 1.93 \times 10^{-4}$). As expected, we also found a highly significant interaction between the factors *Session* (IFC vs. vertex) and *Stimulation* (post vs. pre; $F(202.03) = 11.53$, $p = 8.25 \times 10^{-4}$), a main effect of *Stimulation* ($F(202.03) = 4.85$, $p = 0.03$), but no main effect of *Session* ($F(202.03) = 0.12$, $p = 0.73$). Importantly, we did not observe any two-way interactions between the factors *Exposure* and *Session* ($F(202.03) = 0.03$, $p = 0.87$) or *Stimulation* ($F(28.01) = 3.73 \times 10^{-3}$, $p = 0.95$) and no three-way interaction ($F(202.03) = 0.28$, $p = 0.59$). This argued for the independence of the effects of exposure from TMS-related changes in conscious experience ($BF_{10} = 26.33$). **D. Effects of TMS on phase duration.** Here, we display phase duration collapsed across the two factors *Stimulation* (post vs. pre) and *Session* (IFC vs. vertex) in E3. Phase durations showed no main effect of *Stimulation* ($F(87) = 2.47$, $p = 0.12$, $BF_{10} = 0.49$) and no main effect of *Session* ($F(87) = 0.11$, $p = 0.74$, $BF_{10} = 0.2$). As expected, we found a highly significant between-factor interaction ($F(87) = 6.35$, $p = 0.01$, $BF_{10} = 3.75$), reflecting the relative prolongation of phase duration after TMS to IFC (see Figure 4A).

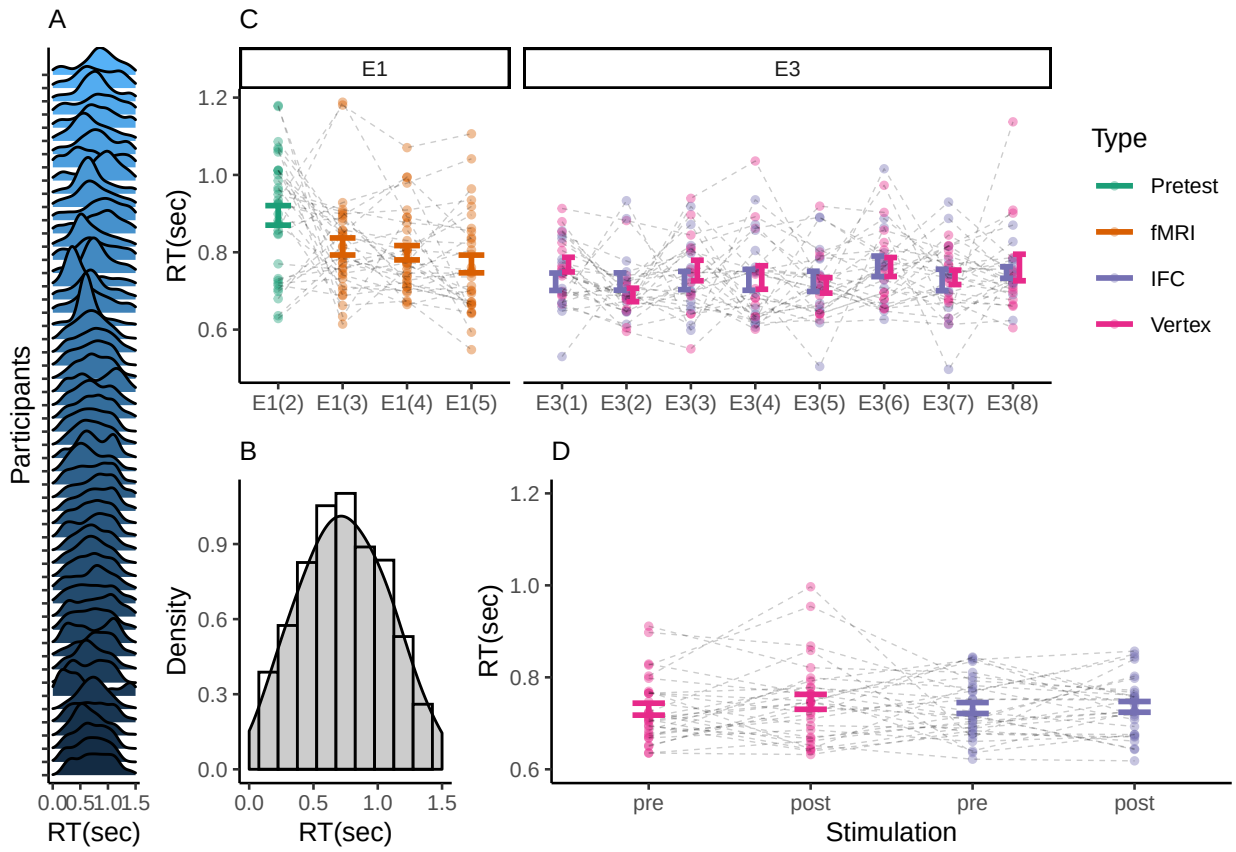

Supplementary Figure S3. Response Times. A. Discontinuous bistable perception. Here, we depict the distribution of RTs for the report of changes in conscious experience in individual participants across E1, E2 and E3. Timepoints are displayed relative to the onset of the preceding overlap. Response times were distributed non-uniformly across the inter-overlap interval (chi-square test against uniformity: $p < 0.05$ in 55 of 55 participants). This ensured that changes in conscious experience were indeed confined to overlapping stimulus configurations, indicating that conscious experience unfolded in a discrete sequence of *perceptual states*. **B. Collapsed RTs.** Across participants, aggregated RTs (0.81 ± 0.05 sec) were best fit by a normal distribution (BIC $= 1.77 \times 10^4$, mean $= 0.74$, sd $= 0.33$) as compared to a gamma (BIC $= 2.1 \times 10^4$) or a lognormal distribution (BIC $= 2.8 \times 10^4$). **C. Effects of stimulus exposure on RTs.** Across the experimental runs of E1 and E3, prolongated exposure to structure-from-motion was associated with a reduction in response times ($F(328.25) = 9.29$, $p = 1.55 \times 10^{-14}$). **D. Effects of TMS on RTs.** In E3, RTs did

not vary according to the factors *Stimulation* (post vs. pre; F(58) = 0.99, p = 0.32, BF_{10} = 0.26) and *Session* (IFC vs. vertex; F(58) = 0.07, p = 0.8, BF_{10} = 0.21). Importantly, we did not observe a significant between-factor interaction (F(58) = 0.52, p = 0.47, BF_{10} = 0.34, see also Figure 4C).

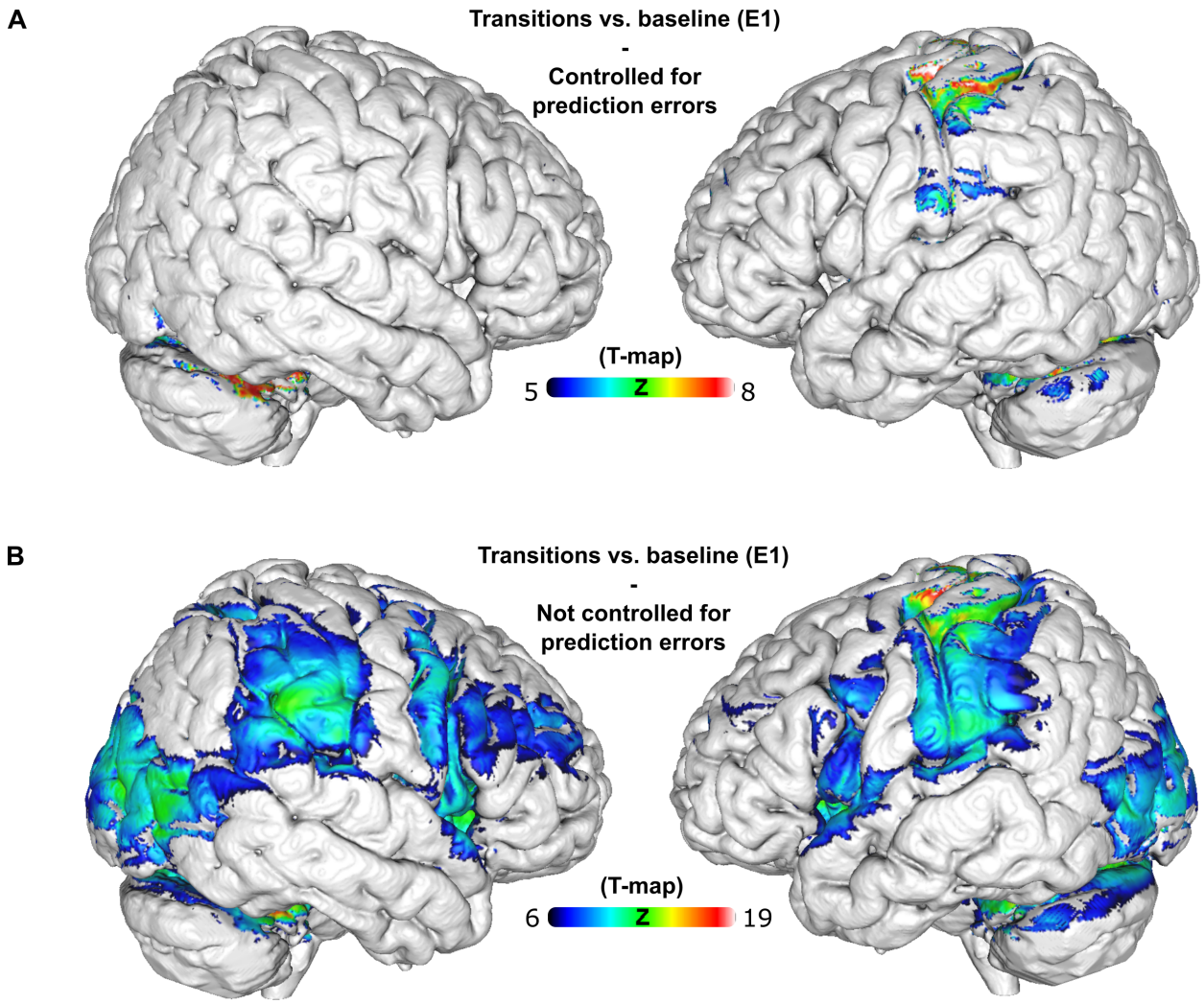

Supplementary Figure S4. The neural correlates of reported changes in perception. A. Controlled for perceptual prediction errors. When analyzing the neural correlates of perceptual events while controlling for BOLD activity related to gradually accumulating perceptual prediction errors (GLM-PC), we found activations in bilateral cerebellum, left pre- and postcentral gyrus, bilateral midcingulate cortex and putamen, left insula, left IPL as well as left medial frontal gyrus ($p_{FWE} = 0.05$). No significant clusters were observed in right-hemispheric IFC or V5/hMT+. **B. Not controlled for perceptual prediction errors.** When assessing the neural correlates of perceptual events without controlling for perceptual prediction errors (i.e., by deleting the prediction-error regressor from GLM-PC), we observed highly significant change-related activity in bilateral insula,

right inferior frontal gyrus, bilateral V5/hMT+, bilateral cerebellum, left pre- and postcentral gyrus, bilateral midcingulate cortex, bilateral inferior parietal lobulus and left middle frontal gyrus ($p_{FWE} = 10^{-6}$). Hence, when studied in isolation of perceptual prediction errors, perceptual events did activate regions in right IFC (see Supplementary Figure S5 for a comparison of the explanatory power of change-related regressors and accumulating perceptual prediction errors with respect to BOLD activity).

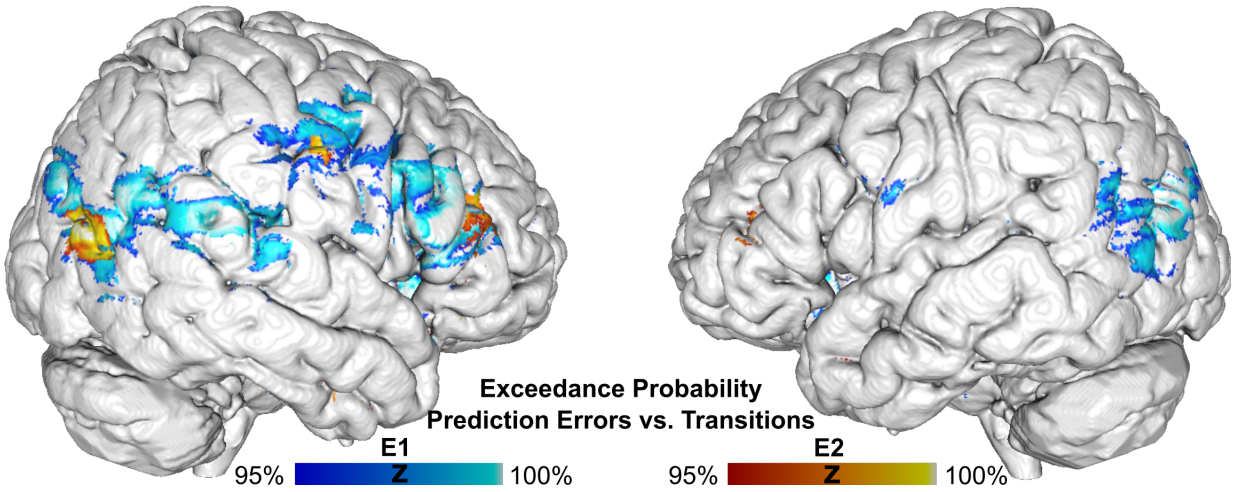

Supplementary Figure S5. Posterior probability maps. We applied a Bayesian Posterior Probability Maps approach to compare the explanatory power of gradually accumulating perceptual prediction errors against the explanatory power of event-related regressors. Here, we display voxels where BOLD activity was better explained by gradually accumulating prediction errors at an exceedance probability above 95% (E1: blue heatmap; E2: red heatmap). Across both experiments, the posterior probability maps yielded converging evidence that neural signals from IFC and V5/hMT+ (as well as from additional parietal brain regions) were better explained by prediction-error related activity as compared to change-related activity.

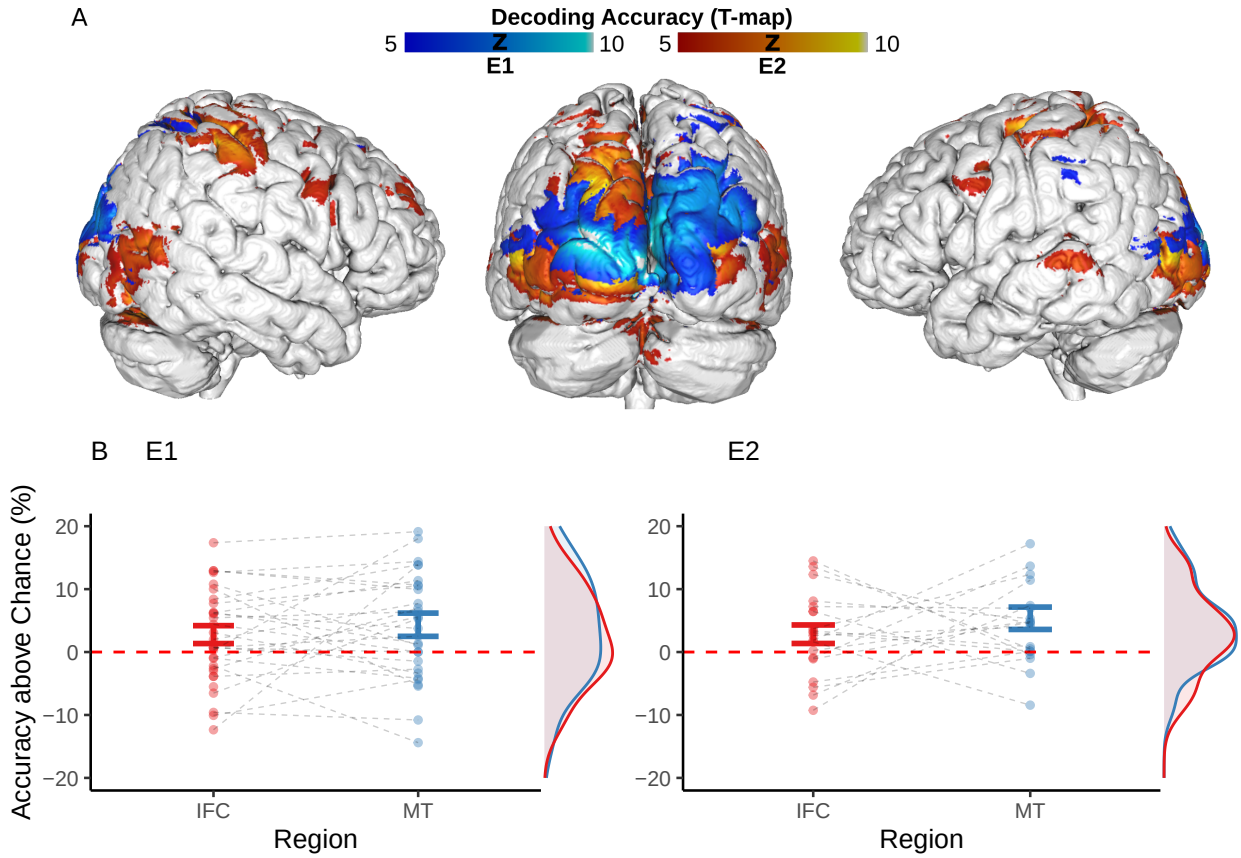

Supplementary Figure S6. Decoding the contents of conscious experience. A. Whole-brain searchlight. Multi-variate pattern analysis of BOLD-data suggested that information about the current content of conscious experience was pre-dominantly represented in posterior brain regions such as visual cortex (including V5/hMT+) and parietal cortex (SPL and IPL). **B. Decoding accuracy in hMT and IFC.** In E1 (left panel), classification accuracy was significantly above chance in V5/hMT+ (T(31) = 2.35, p = 0.03, BF_{10} = 2.03). For IFC, we did not find conclusive evidence for above-chance classification (T(31) = 1.95, p = 0.06, BF_{10} = 1). Likewise, in E2 (right panel), we were able to decode the current contents of conscious experience from V5/hMT+ (T(19) = 3.02, p = 6.97×10^{-3}, BF_{10} = 6.93). E2 yielded no conclusive evidence for above-chance classification in IFC (T(19) = 1.92, p = 0.07, BF_{10} = 1.08).

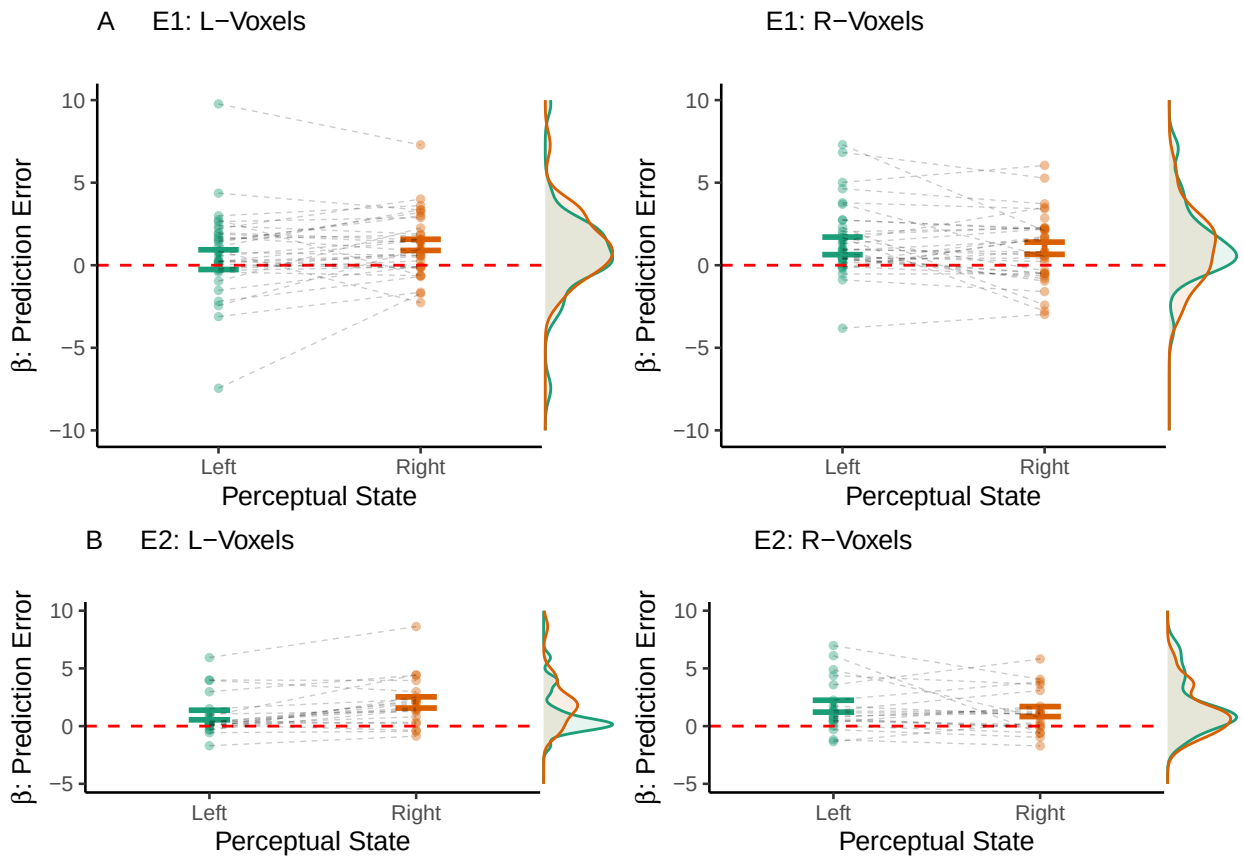

Supplementary Figure S7. Perceptual prediction errors in voxels with reduced biases. A. Experiment E1. As shown above, voxels with biases toward one perceptual interpretation (T > 1) represented perceptual conflict more strongly when the corresponding perceptual interpretation was suppressed. Here, we show that this finding depended on the *strength* of voxel biases. To this end, we selected voxels with reduced biases toward left- or rightward illusory rotation (0 < T < 0.5). In these voxel populations, we re-tested the correlation of BOLD activity with perceptual prediction errors. In this analysis, the representation of perceptual states was not dissociated from the representation of perceptual conflict (L-voxels: T(32) = -1.83, p = 0.08, BF_{10} = 0.83; R-voxels: T(32) = 0.27, p = 0.79, BF_{10} = 0.19). **B. Experiment E2.** Again, we found no consistent evidence for a dissociation between the representation of perceptual states and representation of perceptual conflict in voxels with reduced biases (L-voxels: T(19) = -4.04, p = 7.01×10^{-4}, BF_{10} = 49.88; R-voxels: T(19) = 0.98, p = 0.34, BF_{10} = 0.36).

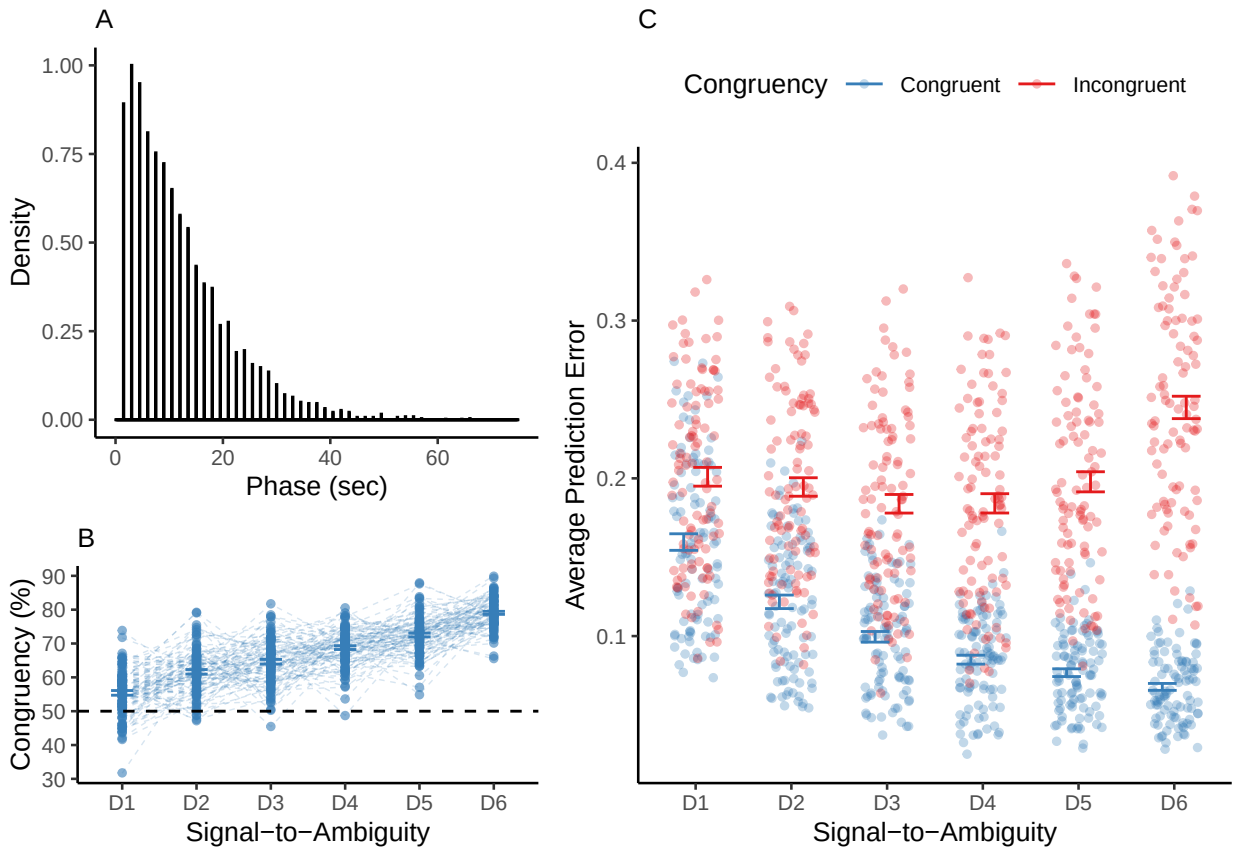

Supplementary Figure S8. Simulating from the predictive-coding model of bistable perception. A. Phase duration. For ambiguous visual stimulation in 100 simulated participants, phase durations were distributed in a sharp rise and long tail. This pattern, which is typical for bistable perception, was best fit by a gamma distribution with a shape parameter of 1.66 and a rate parameter of 0.14 (BIC $= 3.83 \times 10^4$). **B. Graded ambiguity.** During graded ambiguity, disambiguating stimulus information biased simulated conscious experience toward congruent perceptual states. In analogy to our behavioral results, this simulated congruency effect was stronger at higher levels of signal-to-ambiguity ($F(495) = 195.1$, $p = 1.49 \times 10^{-114}$, $BF_{10} = 4.23 \times 10^{120}$). **C. Average prediction errors.** When simulating graded ambiguity, we found that prediction errors were elevated during incongruent as opposed to congruent perceptual states (main effect of *Congruency*: $F(1.09 \times 10^3) = 4.15 \times 10^3$, $p = 0$, $BF_{10} = 6.7 \times 10^{275}$). In analogy to our behavioral results, the modulation of simulated perceptual conflict was enhanced at higher signal-to-ambiguity

ratios (interaction between *Congruency* and *Signal-to-Ambiguity*: $F(1.09 \times 10^3) = 148.71$, $p = 2.1 \times 10^{-120}$, $BF_{10} = 1.97 \times 10^{116}$). In contrast to our behavioral results, we also observed a main effect of *Signal-to-Ambiguity* ($F(1.09 \times 10^3) = 81.43$, $p = 1.07 \times 10^{-72}$, $BF_{10} = 1.14 \times 10^{42}$).

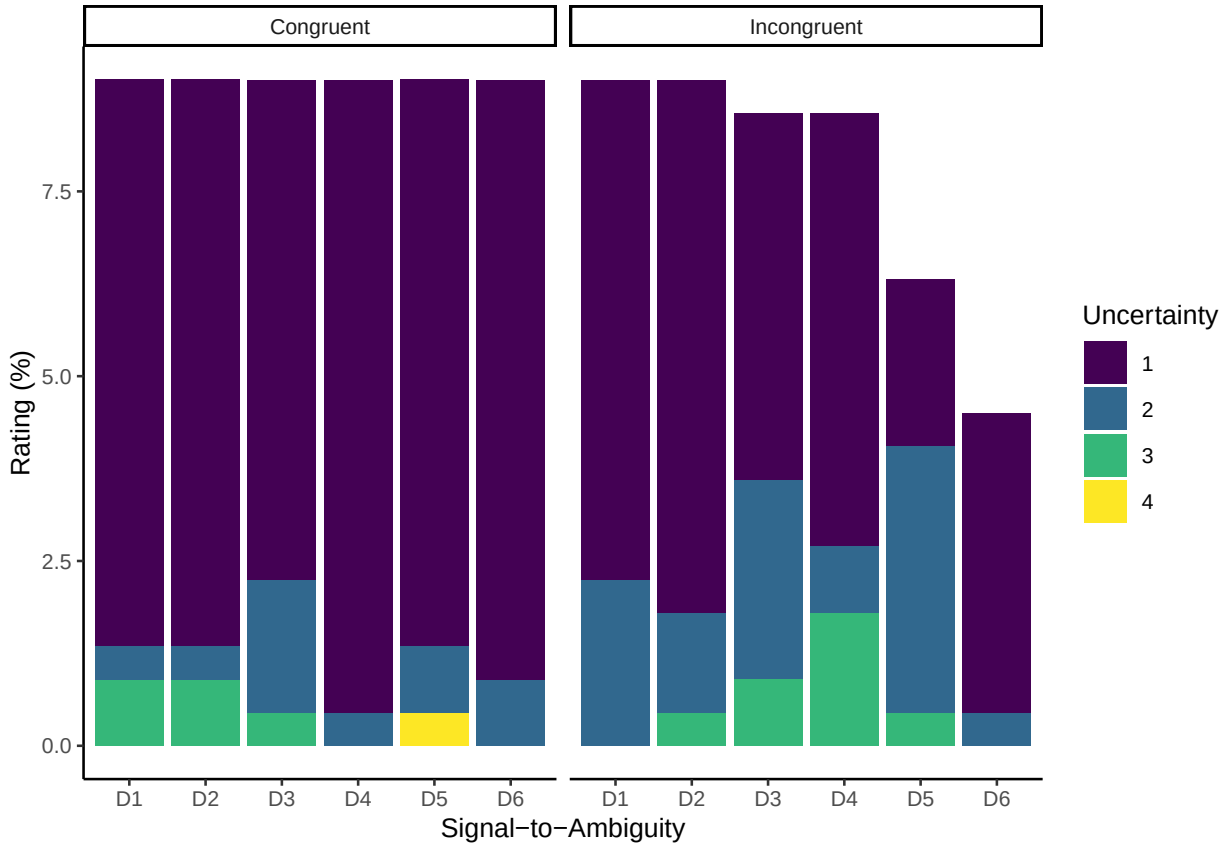

Supplementary Figure S9. Perceptual uncertainty in E2. In the Run 3 of E2, participants viewed one run of graded ambiguity (six levels of signal-to-ambiguity D1-D6, each in one block of 120 sec visual stimulation) and indicated whether they perceived leftward, rightward and unclear direction of rotation of the illusory sphere. In each block, we interrupted visual stimulation at random timepoints during both congruent and incongruent perceptual states. Participants rated perceptual uncertainty on a four-point scale (1: completely certain, 2: rather certain, 3: rather uncertain, 4: completely uncertain). Uncertainty ratings were low during both congruency (average rating: 1.2 ± 0.05) and incongruency (1.4 ± 0.06) to disambiguating stimulus information. Ordinal repeated-measures ANOVA indicated a main effect of *Congruency* (Chi-square = 19.43, p = 3.5×10^{-3}, $BF_{10} = 27.3$). Uncertainty ratings did not vary significantly with *Signal-to-Ambiguity* (Chi-square = 18.19, p = 0.05, $BF_{10} = 2.99 \times 10^{-4}$). Importantly, we also did not find an interaction between *Congruency* and *Signal-to-Ambiguity* (Chi-square = 7.41, p = 0.19, $BF_{10} = 5.53 \times 10^{-5}$). This argued against

differences in perceptual uncertainty as a potential confound in our analysis of the neural correlates of graded ambiguity.

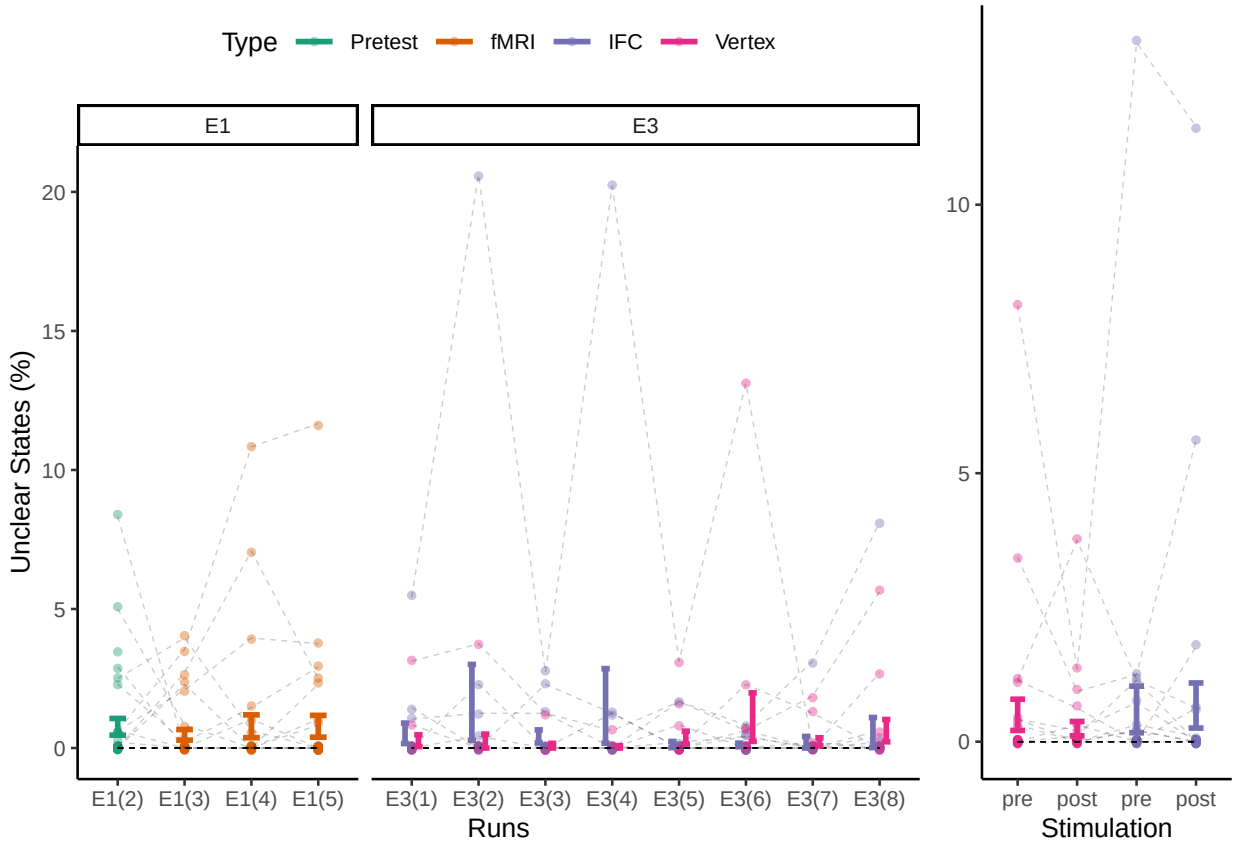

Supplementary Figure S10. Unclear Perceptual States. Across E1 and E3, the frequency of unclear perceptual states did not vary with prolongated stimulus exposure (F(328.79) = 0.72, p = 0.72; left panel). In E3, we found no main effect of *Stimulation* (post vs. pre; F(58) = 0.35, p = 0.56, $BF_{10} = 0.24$), no main effect of *Session* (IFC vs. vertex; F(58) = 0.34, p = 0.56, $BF_{10} = 0.49$) and no between-factor interaction (F(58) = 1.12, p = 0.3, $BF_{10} = 0.31$; right panel).

References

1. Michel, M. *et al.* Opportunities and challenges for a maturing science of consciousness. *Nature Human Behaviour* **3**, 104–107 (2019).

2. Sohn, E. Decoding the neuroscience of consciousness. *Nature* **571**, S2——S5 (2019).

3. Dehaene, S., Lau, H. & Kouider, S. What is consciousness, and could machines have it? *Science* **358**, 486–492 (2017).

4. Koch, C., Massimini, M., Boly, M. & Tononi, G. Posterior and anterior cortex — where is the difference that makes the difference? *Nature Reviews Neuroscience* **17**, 666 (2016).

5. Sandberg, K., Frässle, S. & Pitts, M. Future directions for identifying the neural correlates of consciousness. *Nature Reviews Neuroscience* **17**, 666–666 (2016).

6. Odegaard, B., Knight, R. T. & Lau, H. Should a Few Null Findings Falsify Prefrontal Theories of Conscious Perception? *The Journal of Neuroscience* **37**, 9593–9602 (2017).

7. Boly, M. *et al.* Are the Neural Correlates of Consciousness in the Front or in the Back of the Cerebral Cortex? Clinical and Neuroimaging Evidence. *The Journal of Neuroscience* **37**, 9603–9613 (2017).

8. Baars, B. J. Global workspace theory of consciousness: Toward a cognitive neuroscience of human experience. *Progress in Brain Research* **150**, 45–53 (2005).

9. Dehaene, S. & Changeux, J. P. Experimental and Theoretical Approaches to Conscious Processing. *Neuron* **70**, 200–227 (2011).

10. Lau, H. & Rosenthal, D. Empirical support for higher-order theories of conscious awareness. *Trends in Cognitive Sciences* **15**, 365–373 (2011).

11. Lamme, V. A. Towards a true neural stance on consciousness. *Trends in Cognitive Sciences* **10**, 494–501 (2006).

12. Aru, J., Bachmann, T., Singer, W. & Melloni, L. Distilling the neural correlates of

consciousness. *Neuroscience and Biobehavioral Reviews* **36**, 737–746 (2012).

13. De Graaf, T. A., Hsieh, P. J. & Sack, A. T. The 'correlates' in neural correlates of consciousness. *Neuroscience and Biobehavioral Reviews* **36**, 191–197 (2012).

14. Tsuchiya, N., Wilke, M., Frässle, S. & Lamme, V. A. No-Report Paradigms: Extracting the True Neural Correlates of Consciousness. *Trends in Cognitive Sciences* **19**, 757–770 (2015).

15. Brascamp, J., Sterzer, P., Blake, R. & Knapen, T. Multistable Perception and the Role of the Frontoparietal Cortex in Perceptual Inference. *Annual Review of Psychology* **69**, 77–103 (2018).

16. Blake, R. & Logothetis, N. K. Visual competition. *Nature Reviews Neuroscience* **3**, 13–21 (2002).

17. Leopold, D. A. & Logothetis, N. K. Multistable phenomena: changing views in perception. *Trends in Cognitive Sciences* **3**, 254–264 (1999).

18. Helmholtz, H. von. *Handbuch der Physiologischen Optik.* (Voss, 1867).

19. Sterzer, P., Kleinschmidt, A. & Rees, G. The neural bases of multistable perception. *Trends in cognitive sciences* **13**, 310–8 (2009).

20. Hohwy, J., Roepstorff, A. & Friston, K. Predictive coding explains binocular rivalry: an epistemological review. *Cognition* **108**, 687–701 (2008).

21. Lumer, E. D., Friston, K. J. & Rees, G. Neural correlates of perceptual rivalry in the human brain. *Science (New York, N.Y.)* **280**, 1930–4 (1998).

22. Sterzer, P. & Kleinschmidt, A. A neural basis for inference in perceptual ambiguity. *Proceedings of the National Academy of Sciences of the United States of America* **104**, 323–328 (2007).

23. Weilnhammer, V., Stuke, H., Hesselmann, G., Sterzer, P. & Schmack, K. A predictive

coding account of bistable perception - a model-based fMRI study. *PLOS Computational Biology* **13**, e1005536 (2017).

24. Weilnhammer, V. A., Ludwig, K., Hesselmann, G. & Sterzer, P. Frontoparietal cortex mediates perceptual transitions in bistable perception. *The Journal of neuroscience : the official journal of the Society for Neuroscience* **33**, 16009–15 (2013).

25. Knapen, T., Ee, R. van & Blake, R. Stimulus Motion Propels Traveling Waves in Binocular Rivalry. *PLoS ONE* **2**, e739 (2007).

26. Knapen, T., Brascamp, J., Pearson, J., Ee, R. van & Blake, R. The Role of Frontal and Parietal Brain Areas in Bistable Perception. *Journal of Neuroscience* **31**, 10293–10301 (2011).

27. Frässle, S., Sommer, J., Jansen, A., Naber, M. & Einhäuser, W. Binocular rivalry: frontal activity relates to introspection and action but not to perception. *The Journal of neuroscience : the official journal of the Society for Neuroscience* **34**, 1738–47 (2014).

28. Brascamp, J., Blake, R. & Knapen, T. Negligible fronto-parietal BOLD activity accompanying unreportable switches in bistable perception. *Nature neuroscience* **18**, 1672–1678 (2015).

29. Zou, J., He, S. & Zhang, P. Binocular rivalry from invisible patterns. *Proceedings of the National Academy of Sciences of the United States of America* **113**, 8408–8413 (2016).

30. Pastukhov, A., Vonau, V. & Braun, J. Believable change: bistable reversals are governed by physical plausibility. *Journal of vision* **12**, (2012).

31. Lee, T. S. & Mumford, D. Hierarchical Bayesian inference in the visual cortex. *Journal of the Optical Society of America. A, Optics, image science, and vision* **20**, 1434–48 (2003).

32. Knill, D. C. & Pouget, A. The Bayesian brain: the role of uncertainty in neural coding and computation. *Trends Neurosci.* **27**, 712–719 (2004).

33. Friston, K. A theory of cortical responses. *Philos. Trans. R. Soc. Lond., B, Biol. Sci*

360, 815–836 (2005).

34. Hohwy, J. Attention and conscious perception in the hypothesis testing brain. *Frontiers in psychology* **3**, 96 (2012).

35. Clark, A. Whatever next? Predictive brains, situated agents, and the future of cognitive science. *The Behavioral and brain sciences* **36**, 181–204 (2013).

36. Rosa, M. J., Bestmann, S., Harrison, L. & Penny, W. Bayesian model selection maps for group studies. *NeuroImage* **49**, 217–24 (2010).

37. Heekeren, H. R., Marrett, S., Bandettini, P. A. & Ungerleider, L. G. A general mechanism for perceptual decision-making in the human brain. *Nature* **431**, 859–862 (2004).

38. Born, R. T. & Bradley, D. C. Structure and Visual Function of Area MT. *Annual Review of Neuroscience* **28**, 157–189 (2005).

39. Krug, K., Cicmil, N., Parker, A. J. & Cumming, B. G. A causal role for V5/MT neurons coding motion-disparity conjunctions in resolving perceptual ambiguity. *Current Biology* **23**, 1454–1459 (2013).

40. Haynes, J. D. & Rees, G. Decoding mental states from brain activity in humans. *Nature Reviews Neuroscience* **7**, 523–534 (2006).

41. Arnold, D. H. Why is Binocular Rivalry Uncommon? Discrepant Monocular Images in the Real World. *Frontiers in Human Neuroscience* **5**, 116 (2011).

42. Kersten, D., Mamassian, P. & Yuille, A. Object Perception as Bayesian Inference. *Annual Review of Psychology* **55**, 271–304 (2004).

43. Weilnhammer, V. *et al.* Psychotic Experiences in Schizophrenia and Sensitivity to Sensory Evidence. *Schizophrenia bulletin* (2020). doi:10.1093/schbul/sbaa003

44. Huang, Y. Z., Edwards, M. J., Rounis, E., Bhatia, K. P. & Rothwell, J. C. Theta burst stimulation of the human motor cortex. *Neuron* **45**, 201–206 (2005).

45. O'Shea, J. & Walsh, V. Transcranial magnetic stimulation. **17**, R196–R199 (2007).

46. Wilson, H. R. Minimal physiological conditions for binocular rivalry and rivalry memory. *Vision research* **47**, 2741–50 (2007).

47. Klink, P. C. *et al.* Early interactions between neuronal adaptation and voluntary control determine perceptual choices in bistable vision. *Journal of Vision* **8**, 16 (2008).

48. Van Loon, A. M. *et al.* GABA shapes the dynamics of bistable perception. *Current Biology* **23**, 823–827 (2013).

49. Blake, R., Sobel, K. V. & Gilroy, L. A. Visual motion retards alternations between conflicting perceptual interpretations. *Neuron* **39**, 869–878 (2003).

50. Pastukhov, A. & Braun, J. Cumulative history quantifies the role of neural adaptation in multistable perception. *Journal of Vision* **11**, 12 (2011).

51. Moreno-Bote, R., Knill, D. C. & Pouget, A. Bayesian sampling in visual perception. *Proceedings of the National Academy of Sciences of the United States of America* **108**, 12491–6 (2011).

52. Baldauf, D. & Desimone, R. Neural mechanisms of object-based attention. *Science* **344**, 424–427 (2014).

53. Xu, H. *et al.* Rivalry-like neural activity in primary visual cortex in anesthetized monkeys. *Journal of Neuroscience* **36**, 3231–3242 (2016).

54. Dwarakanath, A. *et al.* Prefrontal state fluctuations control access to consciousness. *bioRxiv* 2020.01.29.924928 (2020). doi:10.1101/2020.01.29.924928

55. Sterzer, P. & Kleinschmidt, A. Anterior insula activations in perceptual paradigms: often observed but barely understood. *Brain structure & function* **214**, 611–22 (2010).

56. Corbetta, M., Patel, G. & Shulman, G. L. The Reorienting System of the Human Brain: From Environment to Theory of Mind. **58**, 306–324 (2008).

57. Opitz, B., Rinne, T., Mecklinger, A., Von Cramon, D. Y. & Schröger, E. Differential contribution of frontal and temporal cortices to auditory change detection: FMRI and ERP results. *NeuroImage* **15**, 167–174 (2002).

58. Garrido, M. I., Kilner, J. M., Stephan, K. E. & Friston, K. J. The mismatch negativity: A review of underlying mechanisms. *Clinical Neurophysiology* **120**, 453–463 (2009).

59. Wessel, J. R., Conner, C. R., Aron, A. R. & Tandon, N. Chronometric electrical stimulation of right inferior frontal cortex increases motor braking. *Journal of Neuroscience* **33**, 19611–19619 (2013).

60. Aron, A. R., Robbins, T. W. & Poldrack, R. A. Inhibition and the right inferior frontal cortex: One decade on. *Trends in Cognitive Sciences* **18**, 177–185 (2014).

61. Bastos, A. M. *et al.* Canonical microcircuits for predictive coding. *Neuron* **76**, 695–711 (2012).

62. Sterzer, P. *et al.* The Predictive Coding Account of Psychosis. *Biological Psychiatry* **84**, 634–643 (2018).

63. Corlett, P. R. *et al.* Hallucinations and Strong Priors. *Trends in Cognitive Sciences* **23**, 114–127 (2019).

64. Sommer, I. E. C. *et al.* Auditory verbal hallucinations predominantly activate the right inferior frontal area. *Brain : a journal of neurology* **131**, 3169–77 (2008).

65. Powers, A. R., Mathys, C. & Corlett, P. R. Pavlovian conditioning–induced hallucinations result from overweighting of perceptual priors. *Science* **357**, 596–600 (2017).

66. Marzouk, T., Winkelbeiner, S., Azizi, H., Malhotra, A. K. & Homan, P. Transcranial Magnetic Stimulation for Positive Symptoms in Schizophrenia: A Systematic Review. *Neuropsychobiology* 1–13 (2019). doi:10.1159/000502148

67. Brainard, D. H. The Psychophysics Toolbox. *Spatial vision* **10**, 433–6 (1997).

68. Morgan, M. J. & Thompson, P. Apparent motion and the Pulfrich effect. *Perception* **4**, 3–18 (1975).

69. Eickhoff, S. B. *et al.* A new SPM toolbox for combining probabilistic cytoarchitectonic maps and functional imaging data. *NeuroImage* **25**, 1325–35 (2005).

70. Rossini, P. M. *et al.* Non-invasive electrical and magnetic stimulation of the brain, spinal cord, roots and peripheral nerves: Basic principles and procedures for routine clinical and research application: An updated report from an I.F.C.N. Committee. *Clinical Neurophysiology* **126**, 1071–1107 (2015).

71. Schicktanz, N. *et al.* Continuous theta burst stimulation over the left dorsolateral prefrontal cortex decreases medium load working memory performance in healthy humans. *PloS one* **10**, e0120640 (2015).

72. Suppa, A. *et al.* Theta burst stimulation induces after-effects on contralateral primary motor cortex excitability in humans. *Journal of Physiology* **586**, 4489–4500 (2008).

73. Valchev, N., Tidoni, E., Hamilton, A. F. de C., Gazzola, V. & Avenanti, A. Primary somatosensory cortex necessary for the perception of weight from other people's action: A continuous theta-burst TMS experiment. *NeuroImage* **152**, 195–206 (2017).

74. Weilnhammer, V. A., Ludwig, K., Sterzer, P. & Hesselmann, G. Revisiting the Lissajous figure as a tool to study bistable perception. *Vision research* **98**, 107–12 (2014).

75. Friston, K. J. & Stephan, K. E. Free-energy and the brain. *Synthese* **159**, 417–458 (2007).

76. Hebart, M. N., Goergen, K. & Haynes, J.-D. The Decoding Toolbox (TDT): a versatile software package for multivariate analyses of functional imaging data. *Frontiers in Neuroinformatics* **8**, 88 (2015).

77. Cortes, C. & Vapnik, V. Support-vector networks. *Machine Learning* **20**, 273–297 (1995).

78. Suzuki, S. & Grabowecky, M. Long-Term Speeding in Perceptual Switches Mediated by Attention-Dependent Plasticity in Cortical Visual Processing. *Neuron* **56**, 741–753 (2007).

79. Ostermann, T., Willich, S. N. & Lüdtke, R. Regression toward the mean – a detection method for unknown population mean based on Mee and Chua's algorithm. *BMC Medical Research Methodology* **8**, 52 (2008).